A neuronal pathway for the supraspinal relay of warm and cool sensation

Authors: Xinying Zhang[1,2], Farin Bourojeni[1], Samuel Ferland[3], Anna McFarlane[4], Kieran A. Boyle[5], Madoka Koyanagi[6], Marie-Eve Paquet[3], Andrew J. Todd[4], Junichi Hachisuka[4], Yves De Koninck[3,5], Feng Wang[3,6 *], Artur Kania[1,2,7,8 *]

Affiliations:

[1]Institut de recherches cliniques de Montréal (IRCM), Montréal, QC, Canada

[2]Integrated Program in Neuroscience, McGill University, Montréal, QC, Canada

[3]CERVO Brain Research Centre, Université Laval, Québec, QC, Canada

[4]University of Dundee, Dundee, UK

[5]School of Psychology & Neuroscience, University of Glasgow, Glasgow, United Kingdom

[6]Department of Medical Neuropharmacology, School of Pharmacological Sciences, Wakayama Medical University. Japan

[5]Department of Psychiatry and Neuroscience, Université Laval, Québec, QC, Canada

[6]Faculty of Dentistry, Université Laval, Québec, QC, Canada

[7]Division of Experimental Medicine, McGill University, Montréal, QC, Canada

[8]Department of Anatomy and Cell Biology, McGill University, Montréal, QC, Canada

18 *Corresponding authors: Email: artur.kania@ircm.qc.ca; feng.wang@fmd.ulaval.ca

Abstract

Cutaneous thermosensation is a fundamental sense allowing discrimination of external temperature changes and driving adaptive responses essential for survival and well-being. This sensory process begins with the activation of peripheral thermoreceptors, which encode the quality and intensity of thermal stimuli into neuronal activity that is further integrated by spinal cord circuits and relayed to supraspinal centres through the anterolateral tract (ALT). While classical experiments identified thermal responsive ALT neurons in the superficial spinal dorsal horn, the functional logic of innocuous temperature relay remains poorly understood. We show that, in mice, the majority of Phox2a-lineage lamina I ALT are selectively tuned to innocuous warming or cooling, and receive direct inputs from peripheral thermoreceptors. Their genetic ablation, chemogenetic or optogenetic manipulation impaired temperature discrimination. Our findings contrast with the previous finding that the majority of ALT neurons being mechano- and thermo-nociceptive and provide novel evidence for the existence of a large ensemble of genetically defined warming- and cooling- responsive ALT neurons. The large representation of innocuous temperature in supraspinal-relaying ALT neurons indicates substantial spinal amplification of thermal information and underscores the importance of innocuous thermosensation in the ascending sensory pathway.

37 **Main**

38 Mammalian spinal cord ALT neurons serve as a hub for the relay of somatosensory information,
39 including mechanosensation, thermosensation, and nociception[1]. ALT neurons within the lamina I
40 of the spinal dorsal horn respond to a variety of somatosensory stimuli, and classical physiological
41 and morphological studies as well as recent *in vivo* calcium imaging experiments argue for the
42 existence of at least cold-selective, nociceptive, and polymodal subtypes[2-6]. While some
43 thermosensory lamina I ALT neurons populations have been identified based on their response to
44 noxious cold and hot stimuli, the integration and relay of innocuous temperatures, which are
45 encountered far more frequently than hot or cold extremes, remains poorly understood[7-10]. In mice,
46 approximately half of ALT neurons are defined by the embryonic expression of the transcription
47 factor Phox2a. Previous studies demonstrated that a subset of these show increased
48 phosphorylation of ERK (pERK) in response to noxious heat, and are located near the termini of
49 Trpm8 and Trpv1 thermoreceptor afferents in lamina I, suggesting a thermosensory function[11,12].

50

51 **Genetically defined thermosensory ALT neurons**

52 We first examined whether mouse Phox2a lamina I (Phox2a^{lamI}) ALT neurons constitute a distinct
53 subset of all lamina I ALT neurons by assessing their expression of molecular markers. To visualize
54 mouse Phox2a^{lamI} neurons, we produced Phox2a^{tdTomato} mice by crossing *Phox2a::Cre*[11] mice with
55 Cre-dependent tdTomato reporter (*R26:lsl-tdTomato*) mice. To distinguish between Phox2a ALT
56 neurons and non-Phox2a ALT neurons, we took advantage of the fact that essentially all ALT
57 neurons innervate the lateral parabrachial nucleus (lPBN) in rodents[13]. Thus, in *R26:lsl-tdTomato*;

58 *Phox2a::Cre* mice bilaterally injected with retrograde tracer, cholera toxin subunit B (CTB), in the
59 lPBN, Phox2a^{lamI} neurons were co-labelled by tdTomato and CTB, whereas non-Phox2a^{lamI} ALT
60 neurons were only labelled by CTB (Fig. 1a, Extended Data Fig. 1a). First, we examined the
61 expression of the transcription factor Zfhx3, proposed to label all long-range spinal projection
62 neurons, including ALT neurons[14]. As expected, essentially all CTB+ lamina I ALT neurons
63 expressed Zfhx3 (Fig. 1c, f). Next, we investigated protein and mRNA markers of ALT neurons
64 that correlate with their proposed somatosensory functions. NK1R, the receptor of substance P,
65 and Tac1, a gene coding for the precursor protein of substance P, have been the predominant marker
66 of ALT neurons and associated with nociception[15]. Aligning with observations in adult and
67 embryonic mice[11,16], we observed lower levels of NK1R protein, and lower *Tac1* mRNA levels in
68 Phox2a^{lamI} neurons, compared to non-Phox2a^{lamI} ALT neurons (Fig. 1b-f, Extended Data Fig. 1d,
69 e and Supplementary Table 1). Past studies also suggested that ALT neurons can be subdivided by
70 their expression of Calbindin protein and *Tacr1* and *Gpr83* mRNA[17,18]. Of these, we found only
71 *Gpr83* showed preferential expression in Phox2a^{lamI} *versus* non-Phox2a^{lamI} ALT neurons
72 (Extended Data Fig. 1b, c, e and Supplementary Table 1). Since low or no NK1R expression in
73 lamina I ALT neurons has been associated with tuning to cold stimuli[19], and Tac1 expression with
74 mechanical nociception[20-22], we hypothesised that Phox2a lamina I ALT neurons may have a
75 preferential role in thermosensation given their low expression of both NK1R and *Tac1*.

76 To test this idea, we performed functional 2-photon calcium imaging of lumbar Phox2a^{lamI}
77 neurons expressing the GCaMP6s calcium sensor in anesthetized mice (*Phox2a::Cre*; *R26:lsl-*
78 *GCaMP6s*). A feedback-controlled probe was used to stimulate the plantar side of the hindpaw
79 with a series of fast-ramp-and-hold thermal stimuli, covering innocuous cool (20°C and 15°C) to
80 noxious cold (6°C), as well as innocuous warmth (38°C) to noxious heat (43°C and 50°C)

81 temperature ranges, from adaptive temperature at 32°C or 25°C respectively (Fig. 1g, h, Extended
82 Data Fig. 2a)[23]. We identified a total of 62 Phox2a^{lamI} neurons (ten imaging fields in eight animals)
83 that showed robust Ca^{2+} responses to either cooling or warming, or both. Of these, 41.9%
84 responded to cooling only (cooling-selective), 40.3% responded to warming only (warming-
85 selective), and 6.5% responded to all cooling and warming testing temperatures (all-temp-sensitive,
86 Fig. 1i). These observations provide first direct evidence that Phox2a^{lamI} ALT neurons are indeed
87 thermosensory and comprise two largely complementary subsets responding to innocuous cooling
88 or warming.

89 Next, we examined whether Phox2a^{lamI} neurons are preferentially tuned to thermal stimuli
90 by comparing their responses to innocuous cooling and warming versus mechanical stimuli (Fig.
91 1j). Repetitive innocuous brushing and noxious pinching were applied manually to the paw. Of 35
92 Phox2a^{lamI} neurons tested (six fields from five animals), none responded to brush, 12 responded to
93 pinch (on average 35.0% per animal), 16 responded to cooling (on average 41.6% per animal), and
94 19 responded to warming (on average 57.5% per animal), while one responded to none of the four
95 tested stimuli (Fig. 1j, Extended Data Fig. 2c, d). Of the 34 responsive neurons, around half thermal
96 sensitive ones responded to cooling or warming (Fig. 1k), consisting with our observation above
97 (Fig. 1i). Specifically, twenty-four neurons were modality-specific, including six neurons
98 responding only to cooling (cooling-selective), 16 neurons responding only to warming (warming-
99 selective), and only three neurons responding only to pinch (pinch-selective, Fig. 1k). ten neurons
100 were multimodal, where one responded to both cooling and warming, and nine responded to both
101 mechanical and thermal stimuli. Notably, all multimodal pinch-responsive neurons also responded
102 to cooling, and they exhibited much smaller Ca^{2+} responses to pinch comparing to their responses
103 to cooling, suggesting that they are still preferentially tuned to thermal stimuli (Fig. 1l). Together,

104 our results suggest that Phox2a lamina I ALT neurons are preferentially tuned to innocuous cool
105 and warm, but not mechanical stimuli.

106

107 **Cool and warm encoding by Phox2a ALT neurons**

108 We next considered three potential neuronal coding mechanisms of Phox2a^{lamI} neurons across the
109 innocuous and noxious temperature ranges: (1) tuning to specific temperatures and selective
110 recruitment; (2) recruitment of increasing numbers of neurons at more extreme temperatures; or
111 (3) graded response amplitudes to different temperatures (Fig. 2a)[24]. To distinguish between these,
112 we measured the proportion of thermal-responsive Phox2a^{lamI} neurons that were recruited at
113 various temperatures, which were similar within the innocuous and noxious range (Fig. 2b). In
114 addition, of the cooling-selective neurons, most neurons that responded to a specific cooling
115 temperature also responded to other cooling temperatures, and the same was true for warming-
116 selective neurons (Fig. 2c), together suggesting broad and not specific tuning to both cooling and
117 warming in Phox2a^{lamI} neurons. Furthermore, the peak Ca^{2+} changes of Phox2a^{lamI} neurons did not
118 show a graded increase between innocuous and noxious ranges (Fig. 2d), suggesting that these
119 neurons are broadly tuned to innocuous temperatures, and do not encode temperature changes in
120 the noxious range.

121 To elucidate the coding strategy of Phox2a^{lamI} neurons in the innocuous temperature range,
122 we examined their Ca^{2+} responses in a series of step-increments or decrements from the adaptive
123 temperature of 30°C (Fig. 2e). Notably, of 27 neurons examined in total, most responded to small
124 increment or decrement of 2°C. Particularly, 16 cooling-responsive neurons were activated at 28°C

125 and one at 26°C (17 neurons in total), and all warming-responsive neurons were activated at 32°C
126 (13 neurons in total), indicating that Phox2a^{lamI} neurons are highly responsive to temperature
127 changes (Fig. 2f). Moreover, both cooling- and warming-responsive neurons showed graded
128 responses within the innocuous range, and their peak Ca^{2+} changes plateaued within the innocuous
129 range, further arguing for a limited ability of these neurons to encode noxious temperatures (Fig.
130 2d, g). Together, these results demonstrate that Phox2a lamina I ALT neurons are broadly tuned to
131 wide-range cooling or warming, and encode innocuous, but not noxious, temperature changes with
132 graded responses.

133

134 **Thermoreceptor inputs to Phox2a neurons**

135 Cutaneous somatosensory information is transmitted to the spinal cord by primary sensory neurons
136 tuned to one or more specific modalities. We reasoned that thermosensory Phox2a ALT neurons
137 may receive direct inputs from thermoreceptors since a previous study reported that Trpm8 cool-
138 thermoreceptor afferents contact the dendrites of Phox2a^{lamI} neurons[25,26]. Additionally, most
139 thermosensory Phox2a^{lamI} neurons were slow-adapting (Fig. 1h), with their normalized full-width-
140 half-maximum (FWHM) of the calcium response larger than 0.5, echoing the characteristics of
141 slow-adapting (SA) Trpm8+ thermoreceptors (Extended Data Fig. 2b; Trpm8 data not shown)[27].
142 To map direct sensory afferent inputs to Phox2a ALT neurons, we performed monosynaptic
143 retrograde tracing, using an EnvA-pseudotyped, glycoprotein-deleted rabies virus (*EnvA(dG)-*
144 *RabV::mCherry*) injected unilaterally into the lumbar enlargement of mice expressing the EnvA
145 receptor (TVA) in Phox2a ALT neurons (*Phox2a::Cre; hCdx2:FlpO; R26:lsl-fsf-HTB*, Fig. 3a). As
146 expected, the rabies virus selectively infected spinal dorsal horn Phox2a ALT neurons

147 (mCherry+GFP+, starter cells), but not neurons lacking TVA (Fig. 3b, Extended Data Fig 3a, b).
148 Across L3-L5 dorsal root ganglia (DRGs), we observed rabies-infected sensory neurons
149 (mCherry+ and NeuN+), encompassing peptidergic C- and Aδ-fiber populations (TrkA+, CGRP+)
150 known to include thermoreceptors and nociceptors presynaptic to superficial ALT neurons (Fig.
151 3c, d, Extended Data Fig. 3c, d)[1]. Among these, we identified neurons expressing *Trpm8 and Trpv1*
152 mRNAs, markers of cold and hot thermoreceptors, respectively, suggesting direct monosynaptic
153 input from both to Phox2a ALT neurons. Given that Trpm8+ and Trpv1+ afferents terminate
154 predominantly in the superficial dorsal horn[25,26,28], it is likely that these labelling by rabies transfer
155 arise superficially from Phox2a ALT neurons in lamina I rather than deeper layers. In contrast, no
156 non-peptidergic sensory neurons (IB4+) were labelled. However, this result should be interpretated
157 with caution, as this population has well reported to be resistant to rabies infection[29].

158 We next sought electrophysiological evidence of direct synaptic inputs of Trpm8+
159 thermoreceptors onto Phox2a^{lamI} neurons, as previous study demonstrated one subpopulation of
160 Phox2a ALT neurons are selectively contacted by Trpm8 fibers[25]. To do so, we conducted whole-
161 cell patch clamp recordings from these neurons in an *ex vivo* semi-intact somatosensory
162 preparation, comprising the continuum of spinal cord, DRGs, saphenous nerve, femoral nerve, and
163 hindlimb skin[30]. Among the 28 Phox2a^{lamI} neurons examined, the majority (19 neurons) responded
164 selectively to cooling (cool-selective), with action potentials elicited by a drop of 15°C saline
165 applied to the skin (skin temperature change: 32°C to 20°C), but not to warming (50°C saline, skin
166 temperature change: 32°C to 38°C) or noxious mechanical stimulation (4.0 von Frey filament, Fig.
167 3e, Extended Data Fig. 4a). In cool-selective Phox2a^{lamI} ALT neurons (Fig. 3a), spontaneous
168 excitatory post-synaptic currents (EPSCs) were abolished in the presence of tetrodotoxin (TTX)
169 and reinstated in the presence of WS-12, a Trpm8 agonist[31], in addition to TTX. This implied that

170 the Trpm8+ afferents indeed provide monosynaptic inputs to cool-selective Phox2a^{lamI} ALT
171 neurons (Fig. 3b, c). We further asked whether innervation by cold-selective Trpm8+
172 thermoreceptors underlies the cool selectivity of Phox2a^{lamI} neurons. To test this, we utilized
173 *Phox2a::Cre; Trpm8:FlpO; R26:lsl-tdTomato; R26:fsf-EGFP* mice to visualize Phox2a^{lamI}
174 neurons and Trpm8 fibers, such that Phox2a neurons expressed tdTomato and Trpm8 afferents
175 expressed GFP (Fig. 4h). Using the *ex vivo* semi-intact preparation, we recorded the thermal
176 responses of Phox2a^{lamI} neurons in close contact with dense Trpm8 fibers. Strikingly, the vast
177 majority (90%) of the these neurons were either cool-selective or exhibited subthreshold response
178 limited to cooling stimuli (Fig. 3i, Extended Data Fig. 4b), suggesting that Trpm8 innervation is
179 likely indictive of cool selectivity in Phox2a^{lamI} ALT neurons.

180 In addition, anatomical reconstructions of the 28 recorded Phox2a^{lamI} neurons (diI-filled,
181 from recordings in Fig. 3e) revealed that cool-selective and non-cool-selective (mechano-selective
182 and polymodal) neurons exhibited distinct somatic and dendritic features (Fig. 3j, Extended Data
183 Fig. 4c). The cool-selective neurons had smaller soma volume, and less complex dendritic structure
184 featured with fewer branches and lower density in Sholl analysis, and correspondingly shorter
185 total rostro-caudal and medial-lateral dendritic lengths (Fig. 3k, Extended Data Fig. 4d-f). We also
186 performed principal component-based unsupervised hierarchical clustering (HCPC) of the
187 morphological features of these neurons, which revealed two natural clusters that largely
188 corresponded to non-cool-selective and cool-selective physiological profiles (Extended Data Fig.
189 4g). Together, these results suggest that Phox2a^{lamI} ALT neurons comprise two main subgroups
190 that are cool-selective and non-cool-selective and correlated with Trpm8 afferent contacts and
191 specific morphological characteristics.

192

193 **Situating Phox2a ALT neurons in thermosensory circuits**

194 Beyond peripheral thermoreceptors, thermal information is processed by spinal cord interneurons
195 and brain circuits. First, to assess whether local interneurons provide indirect inputs and
196 modulation onto Phox2a ALT neurons, we performed a new set of monosynaptic rabies tracing
197 experiment as our previous approach yielded insufficient labeling of local interneurons. We
198 utilized an optimized helper virus to express TVA in Phox2a neurons and followed by pseudotyped
199 rabies virus infection (Fig. 4a). Among the rabies-infected cells, we identified Phox2a ALT starter
200 neurons as well as interneurons that are directly presynaptic to them (Extended Data Fig. 5a). The
201 majority of superficial lamina I-III interneurons presynaptic to Phox2a neurons were putatively
202 excitatory, as they did not express inhibitory neuronal marker, paired box 2 (PAX2) transcription
203 factor (Extended Data Fig. 5a, b). This aligns with the high sensitivity of Phox2a^{lamI} neurons to
204 cooling or warming, observed in our calcium imaging result (Fig 2f). Nevertheless, we did observe
205 *Kcnip2*+ (inhibitory) and Calbindin+ (excitatory) interneurons, the two subpopulations previously
206 linked with cooling sensation[32,33], as well as *Erbb4*+ (excitatory) interneurons associated with heat
207 sensation (Fig 4b)[34]. Thus, in addition to receiving direct inputs from peripheral thermoceptors,
208 Phox2a ALT neurons may also indirectly receive cool and warm temperature-related information
209 from local interneurons (Fig 4c).

210 We next asked whether supraspinal thermosensory circuits receive direct inputs from
211 Phox2a ALT neurons. Two principal central thermosensory pathways have been proposed: one
212 involves parabrachial neurons projecting to the hypothalamus, primarily the preoptic area (POA),
213 and is implicated in thermoregulatory homeostatic responses. The other includes caudal thalamic

214 neurons, particularly those in the posterior limiting nucleus (PoL), which project to the posterior
215 insular cortex (pIC) for thermal discrimation[10,24]. To determine the relationship between these two
216 pathways and Phox2a ALT neurons, we used *Phox2a::Cre; hCdx2::FlpO; R26:lsl-fsf-*
217 *SynaptophsinGFP* to visualize axonal terminals of Phox2a ALT neurons (GFP+), and labelled
218 POA-projecting lPBN neurons or pIC-projecting PoL neurons by injecting the retrograde tracer
219 CTB-555 in the POA or pIC, respectively (Fig. 4d, f, Extended Data Fig. 5c). We observed synaptic
220 terminals of spinal Phox2a ALT on the soma of POA-projecting PBN neurons, as well as on pIC-
221 projecting PoL neurons, suggesting directly connectivity between Phox2a ALT neurons and both
222 thermosensory pathways (Fig. 4e, g, Extended Data Fig 5d). Together, our circuit tracing
223 experiments position Phox2a ALT neurons to receive theormosensory information both directly
224 from peripheral thermoreceptors and indirectly from spinal networks, and to channel it to
225 thermoregulatory and discriminative neural pathways.

226

227 **Thermoception requires Phox2a ALT neurons**

228 To determine whether Phox2a ALT neurons are functionally required for thermosensation, we
229 selectively expressed diphtheria toxin receptor (DTR) or designer receptors exclusively activated
230 by designer drugs (DREADDs) in spinal Phox2a neurons via the transgenic intersection of
231 *Phox2a::Cre* and *Lbx1:FlpO*. This intersection provided selective access to Phox2a-lineage spinal
232 neurons[35], capturing 45.6% of lamina I neurons versus 18% of those in the deep dorsal horn
233 (Extended Data Fig. 6a). Moreover, Phox2a neurons in the sympathetic or noradrenergic systems
234 were not captured by this intersection[11] (Extended Data Fig. 6b), thereby minimizing off-target
235 effects. First, we ablated adult spinal Phox2a neurons by injecting diphtheria toxin (DTX) into

236 *Phox2a::Cre; Lbx1:FlpO; Tau:lsl-fsf-DTR; R26:fsf-lsl-tdTomato* mice (ablated), or into their
237 control (Ctrl) littermates lacking either *Cre*, *FlpO*, or *DTR* transgenes. Two weeks following DTX
238 injection, compared to the control cohort, the number of tdTomato+ neurons was reduced to 10%
239 in the ablated cohort, and their axon terminals in various brain targets were also ablated (Fig. 5a,
240 b, Extended Data Fig. 6c. Moreover, by bilateral retrograde labelling of all ALT neurons from the
241 lPBN, we confirmed that the ablation reduced by approximately half the number of lamina I ALT
242 neurons without significant effects on other spino-lPBN subpopulations (Extended Data Fig. 6d)[16].
243 Previous studies demonstrated that manipulating thermoreceptor DRG neurons or cool-selective
244 spinal interneurons disrupted temperature discrimination in operant and/or preference task[24,36-38].
245 Therefore, we asked whether a loss of spinal Phox2a ALT neurons would cause a similar phenotype.
246 In two-plate temperature preference test (TPTP), mice chose between two plates held at either a
247 neutral temperature (30°C) or a test temperature (20°C or 38°C). Compared to the control, ablated
248 mice showed a decreased preference for the 38°C plate (Fig. 5c). Similarly, when mice were placed
249 on a thermal gradient, ranging from 7°C to 52°C, ablated mice showed a less sharp temperature
250 preference peak, and a significant decrease of preference in the 37°C zone compared to control
251 mice (Fig. 5d).

252 To investigate the effects of acute manipulation of Phox2a ALT neurons, we selectively
253 expressed hM4Di (inhibitory) or hM3Dq (activating) DREADDs in Phox2a ALT neurons
254 (Extended Data Fig. 7a). Thirty minutes following Clozapine N-oxide (CNO) delivery, similar to
255 DTX-ablated mice, hM4Di-expressing mice also showed disrupted preference in the thermal
256 gradient with reduced preference for the 37°C zone (Fig. 5f). In contrast, hM3Dq-expressing mice
257 showed increased preference of the 38°C plate over 30°C in TPTP (Extended Data Fig. 7d).

258 Therefore, both acute and chronic loss-of-function in Phox2a ALT neurons impaired the thermal
259 preference in mice.

260 Since essentially all Phox2a ALT neurons innervate the lPBN[11,16], we next examined
261 whether optogenetic activation of Phox2a ALT terminals in bilateral lPBN in *Phox2a::Cre;*
262 *hCdx2::FlpO; R26:lsl-fsf-CatCh/EYFP* mice would give rise to similar behavioral phenotypes[39].
263 Like the ablated and chemogenetically-inactivated group, CatCh-expressing mice also showed
264 disrupted thermal preference, shifted towards cooler temperatures with an increased preference in
265 the 25°C zone (Fig. 5h). This suggests that activating warm and cool Phox2a ALT inputs to the
266 lPBN without fine spatial or temporal control may disrupt normal thermal signaling, resembling
267 the effect of input loss. On the other hand, we failed to observe changes in two-plate temperature
268 preference in hM4Di+ and CatCh+ group, or thermogradient preference change in hM3Dq+ group,
269 possibly due to insufficient neuronal activity changes or a plateau effect of preference (Fig. 5e, g,
270 Extended Data Fig. 7e).

271 In addition to the above measurements that assess the perception of innocuous temperature,
272 we also examined nocifensive responses in the above-described mice models. Ablated mice did
273 not differ in their responses to hot or cold plate (Extended Data Fig. 6f), particularly in the latency
274 to flutter or flinch that are largely rubrospinal-driven, and did not differ in mechanical nociception
275 or locomotion (Extended Data Fig. 6g, h)[21]. In contrast, ablated mice unexpectedly showed
276 increased licking response evoked by both cold stimuli through the application of acetone to the
277 plantar surface of a hindpaw, and intraplantar injection of capsaicin, a TRPV1 channel agonist
278 (Extended Data Fig. 6e). Comparably, we also observed increased capsaicin-evoked licking in the
279 hM4Di group, but not following acetone application (Extended Data Fig. 7b, c), and neither in the

280 hM3Dq+ group (Extended Data Fig. 7f, g). We reason that although Phox2a^{lamI} neurons do not
281 directly encode noxious temperature, they likely coordinate with nociceptive, non-Phox2a ALT
282 neurons to drive nocifensive responses towards noxious thermal stimuli and may modulate
283 analgesia through spinal or descending circuits. Together, our results showed that Phox2a ALT
284 neurons are essential for normal thermal perception, but their contribution to nociception,
285 particularly mechanical, is minimal.

286 We next considered whether Phox2a ALT neurons also contribute to thermoregulation-
287 impacting metabolic functions, as previously observed in global Trpm8 knockout mice[40]. The
288 metabolic parameters were largely unchanged in the ablated mice (Extended Data Fig. 8h-k), nor
289 did the core body temperature change in ablation, chemogenetic-inactivation, or optogenetic
290 activation (Extended Data Fig. 9e-g). This largely aligns with the observations in studies
291 specifically ablating the peripheral thermoreceptors[41], indicating that cutaneous thermosensation
292 is dispensable for the gross metabolic function and thermoregulation. However, we did observe an
293 overall increase of loss of water vapor (VH_2O) along with increased water consumption in the
294 male ablated group, similar to metabolic events during heat dissipation[42] (Extended Data Fig. 8a-
295 d). Additionally, ablated male mice also displayed higher food consumption and dark-cycle activity
296 (Extended Data Fig. 8e-g). Unexpectedly, although no difference was found in energy expenditure
297 comparing to the control group, male ablated group showed decreased body weight, and lower fat
298 composition (Extended Data Fig. 9a-d). Some of the observed effects could involve the lPBN-
299 POA circuit given its proposed function in thermoregulation, however, other brain targets of
300 Phox2a ALT neurons involved in autonomic functions such as the nucleus tractus solitarius (NTS),
301 parvicellular reticular nucleus (PARN), and intermediate reticular nucleus (IRN) may also
302 participate in thermoregulation[1,43]. Overall, the presence of these metabolic phenotypes in the

absence of core temperature shifts and major metabolic parameter changes suggests that Phox2a ALT neurons contribute to nuanced autonomic adjustments that are distinct from the primary homeostatic thermoregulatory response.

307 **Discussion**

308 The ALT has been extensively studied for its role in nociception, including noxious mechanical
309 and noxious thermal sensation. Although innocuous thermosensitive ALT neurons, particularly
310 cold-selective ones, have also been identified through electrophysiological recordings, their
311 molecular identity and temperature encoding strategies, particularly in innocuous thermal sensing,
312 remain largely unknown[2,7,19]. We uncovered a neuronal ensemble for innocuous thermal perception,
313 genetically defined by the developmental expression of the transcription factor *Phox2a* and
314 comprising around half of lamina I ALT neurons. Our data show that these neurons constitute the
315 central hub of thermosensation within the central nervous system, receiving directly thermal
316 information from peripheral thermoreceptors and dorsal horn thermosensory interneurons, and
317 relaying it to both discriminative thermosensory and thermoregulatory brain pathways.

318 The existence of central integration and relay of the innocuous thermal information has
319 been implied by recent evidence of large representation of warm and cool neurons in the thalamus
320 and cortex[10,24,44]. Our experiments argue that Phox2a^{lamI} ALT neurons comprise two largely non-
321 overlapping ensembles with preferential tuning to a wide range of warming or cooling
322 temperatures. Given a previous study characterizing all lamina I ALT neurons demonstrated that
323 about half of them responded to cold or warm but not to noxious mechanical stimuli, we infer that
324 the thermal-selective population is likely to be the Phox2a neurons that constitute ~59% of all
325 lamina I ALT neurons, while the non-Phox2a neurons constitute the noxious mechanical selective
326 population[5,11]. Although *in vitro* and *in vivo* functional studies of thermosensory ALT neurons in
327 rodents and cats described few if any warm-tuned ALT neurons, our calcium imaging experiments
328 identified a surprisingly large cohort of them. Several factors may have contributed to their historic

329 underrepresentation, including the low temporal resolution and sensitivity of Fos induction
330 experiments, absence of descending modulation in *in vitro* electrophysiological recordings[45],
331 biased sampling of cool vs. warm ALT cells based on the location of antidromic stimulation or
332 fluorescent intensity of tracers used due to soma size differences[10], and the biased distribution of
333 thermoreceptors in hairy versus glabrous skin in different test conditions[28].

334 Our study provides new insights into the mechanism of thermosensation. Notably, cooling-
335 responsive Phox2a^{lamI} neurons showed similar response properties and temporal dynamics as the
336 Trpm8 sensory neurons: both are slow-adapting and encode innocuous cool temperature in a
337 graded manner. Moreover, many cooling-responsive Phox2a ALT neurons and Trpm8 neurons also
338 showed decreased Ca^{2+} responses during warming, known as the "Cool-ON/Warm-OFF" response
339 type mediated by Trpm8 conductance[46]. Therefore, given their monosynaptic connections, the
340 activity of Phox2a cooling-responsive neurons is likely directly dictated by Trpm8-expressing
341 thermoreceptor neurons. Intriguingly, the proportion of innocuous thermal–responsive Phox2a
342 ALT neurons is much higher than that of thermoceptive DRG neurons, particularly the warm ones,
343 suggesting a substantial amplification at the spinal level[4,23,24]. One hypothesis is that besides
344 receiving direct inputs from TRPV1 hot-thermoreceptors, the activation of warm Phox2a ALT
345 neurons may be subject to feedforward control or disinhibition by local circuits[32-34]. Thus, Phox2a
346 ALT neurons comprising the first central nervous system thermosensory node which can integrate
347 and amplify thermal information, instead of merely relaying it.

348 Prior studies have shown that disruption of periphery thermoreceptors, thalamic nuclei, or
349 the pIC impairs thermal perception[24,36,38] and our experiments demonstrate a similar requirement
350 for Phox2a ALT neurons. On the other hand, although manipulating brain thermoregulatory

351 circuits that receive ALT-relayed information resulted in abnormal thermoregulation[47,48], neither
352 peripheral thermoreceptor deletion, nor our Phox2a ALT ablation resulted in notable
353 thermoregulatory or metabolic defects[41,49]. Thus disrupting cutaneous thermosensation or its relay
354 may be compensated by redundant thermoregulatory pathways involving airways, autonomic
355 nervous system, and/or brown adipose tissue[50]. More generally, our experiments support a model
356 in which discriminatory thermal perception and thermoregulation are processed in parallel and
357 independently[10].

358 In sum, our work provides a foundation for understanding of neural mechanisms of thermal
359 perception, and thermal pain hypersensitivity in pathological conditions. The evolutionary
360 conservation of thermal encoding strategies and Phox2a expression, suggests the transmission of
361 innocuous thermosensory information by cool and warm selective ALT neurons may be part of a
362 global molecular logic of thermosensation[3,8,10,11,45].

363

364

365

366

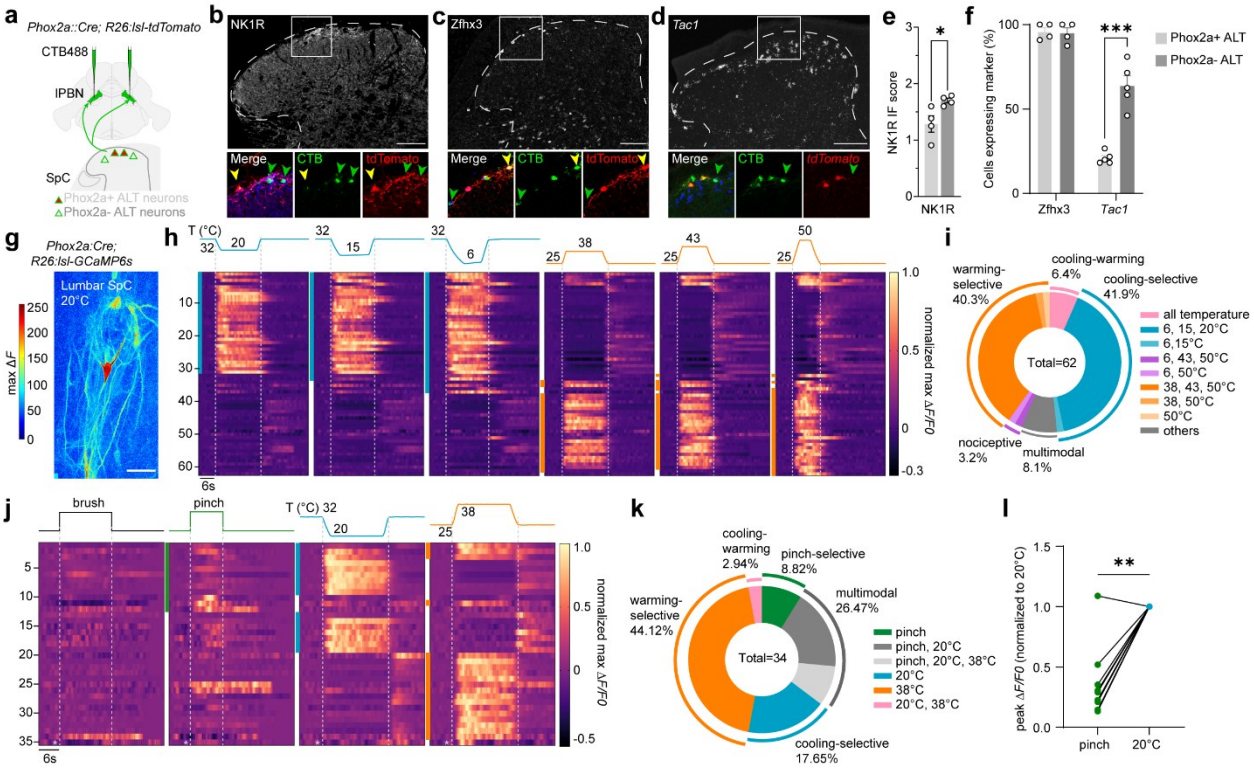

Fig. 1 | Spinal Phox2a^{lamI} ALT neurons form ascending sensory pathway preferentially tuned to temperature. a, Retrograde labelling of ALT neurons by injection of CTB in the bilateral lPBN in *Phox2a::Cre; R26:lsl-tdTomato* mice. **b-d,** Representative images of Phox2a+ (yellow arrowhead) and Phox2a- (green arrowhead) ALT neurons in lumbar spinal cord, labelled with CTB (green) and protein expression of tdTomato (red), and NK1R **(b)** or Zfhx3 (white, **c**) or mRNA expression of *tdTomato* (red) and *Tac1* (white, **d**). **e, f**, Quantification of NK1R expression level **(e)** and fraction of Phox2a+ ALT neurons (light grey) or Phox2a- ALT neurons (dark grey) co-expressing Zfhx3 or Tac1 **(f)**. **g,** Representative imaging field, pseudo coloured based on maximum ΔF of calcium responses to 20°C thermal stimuli in a *Phox2a::Cre; R26:lsl-GCaMP6s* mouse. **h,** Heatmaps of normalized response amplitudes (ΔF/F) to thermal stimuli delivered by a Peltier device: cooling stimuli with baseline temperature of 32°C and decreasing to 20°C, 15°C, or 6°C; warming stimuli with baseline temperature of 25°C and increasing to 38°C, 43°C, or 50°C. Each

380 row represents responses of the same individual neuron (n=62). **i,** Response profile to all thermal
381 stimuli of Phox2a^{lamI} neurons in **(h)**. **j,** Heatmaps of normalized response amplitudes (ΔF/F) to
382 manual brush, pinch, or innocuous thermal stimuli. Each row of the heatmap represents responses
383 of an individual neuron (n=35). **k,** Summary of responses of Phox2a^{lamI} neurons to all stimuli
384 modalities from **(j)**. **l,** Peak calcium signals to pinch of all pinch and 20°C responsive neurons
385 compared to their normalized signals to 20°C. Scale bar: 100 μm in **(b-d) and** 50 μm in **(g)**.
386 Statistics: values plotted as mean ± SEM. N=4 for Zfhx3 and NK1R, N=5 for Tac1, Phox2a+ and
387 Phox2a- ALT neurons. Mean ± SEM. *p <0.05, **p <0.01, ***p < 0.001, non-significant not
388 labelled. Student t-test **(e, f)**, and Paired t-test **(l)**.

389

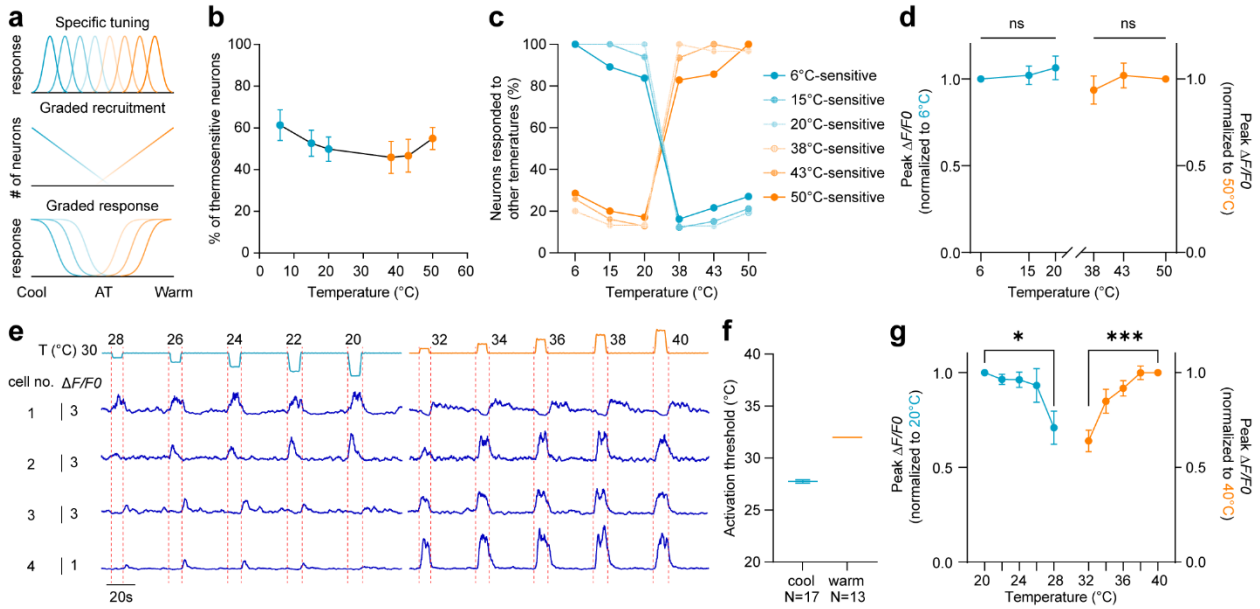

Fig. 2 | Encoding of cool and warm by Phox2a^{lamI} ALT neurons. a, Three possible temperature encoding models adapted from Vestergaard, et al. [24] **b, c,** Percentage of all thermosensory neurons that responded to each thermal stimuli **(b)** and percentage of neurons activated by a given temperature (coloured lines) that responded to each thermal stimuli **(c)** showed broad tuning property. There was no significant difference among the responses to different stimuli. **d,** Thermal-sensitive Phox2a^{LamI} neurons do not exhibit stronger response to noxious thermal stimuli compared to innocuous thermal stimuli. **e,** Representative calcium curves from four neurons showing typical responses to step changes in thermal stimuli with a baseline temperature of 30°C. Cell number 1 responded to warming stimuli and to the return phase of coolinging stimuli. Cell number 2 responded to both cooling and warming stimuli. Cell number 3 and 4 responded to warming stimuli and to the return phase from cooling stimuli. **f,** Activation threshold for the thermal induced calcium responses in cooling or warming responsive cells. **g,** Normalized peak amplitude of wide-range cooling neurons (blue, N=17) and wide-range warming neurons (orange, N=13) to decreasing and increasing temperature, respectively. Mean ± SEM. *p <0.05, **p <0.01, ***p <

405 0.001, ns: non-significant. Ordinary one-way ANOVA **(c)**, Repeated Measurement one-way

406 ANOVA **(d, g)**.

407

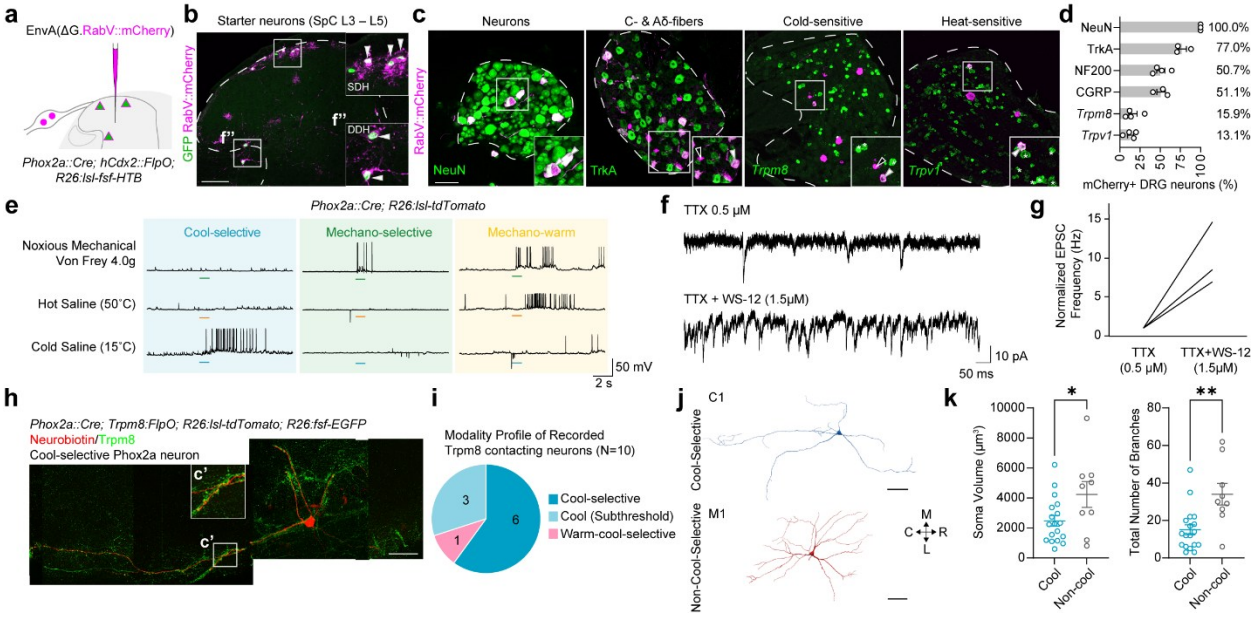

Figure 3 | Evidence of thermoreceptor inputs to Phox2a^{lamI} ALT neurons. a, Rabies tracing with EnvA(ΔG.RabV::mCherry injection in the lumbar cord of *Phox2a::Cre; hCdx2::FlpO; R26:lsl-fsf-HTB* mice. Spinal Phox2a ALT neurons express histone-GFP and rabies infected cells express mCherry. **b,** Representative transverse spinal cord section containing Phox2a starter cells expressing histone-GFP (green) and mCherry (magenta). **c,** Representative images of DRGs containing rabies infected cells (magenta), expressing sensory neuron marker proteins NeuN or TrkA, or *Trpm8* or *Trpv1* mRNAs (green). White arrow: rabies infected cells expressing the marker, open arrow: rabies infected cells not expressing the marker, *: cells expressing the marker not infected by rabies. **d,** Percentage of rabies infected DRG neurons co-expressing a marker over all rabies infected cells (mCherry+ DRG neurons). **e,** Representative traces of a cool-selective cell (blue), mechano-selective cell (green), or a polymodal cell (yellow) with action potentials evoked by cold saline (15°C, blue), or noxious mechanical (4.0g Von Frey filament, green), or hot saline (50°C, orange). Underbars: stimulus onset. **f, g,** Representative traces **(f)** and normalized EPSC frequency **(g)** of cool-selective Phox2a lamina I ALT neurons following the application of 0.5 μM

423 tetrodotoxin (TTX) abolishing spontaneous EPSCs and reinstated in the presence of 1.5 μM WS-
424 12, a Trpm8 agonist, in addition to TTX (n=3). **h,** Tiled image of a neurobiotin-filled cool-selective
425 Phox2a^{lamI} neuron (red) contacted by Trpm8 fibres (green). **i,** Response profiles of recorded
426 Phox2a^{lamI} neurons (n=10), preselected based on their proximity to Trpm8 fibres, with the majority
427 being cool-selective. **j, k,** Representative reconstructed neurobiotin-filled neurons **(j)** post-
428 recording in **(e)** and somatic and dendritic characteristics **(k)** of the cool-selective cells and non-
429 cool-selective cells. Scale bar: 100 μm in **(b, c, h**) and 50 μm in **(j)**. Mean ± SEM. *p <0.05, **p
430 <0.01, ***p < 0.001, non-significant not labelled. Mann-Whitney test in **(k)**.

431

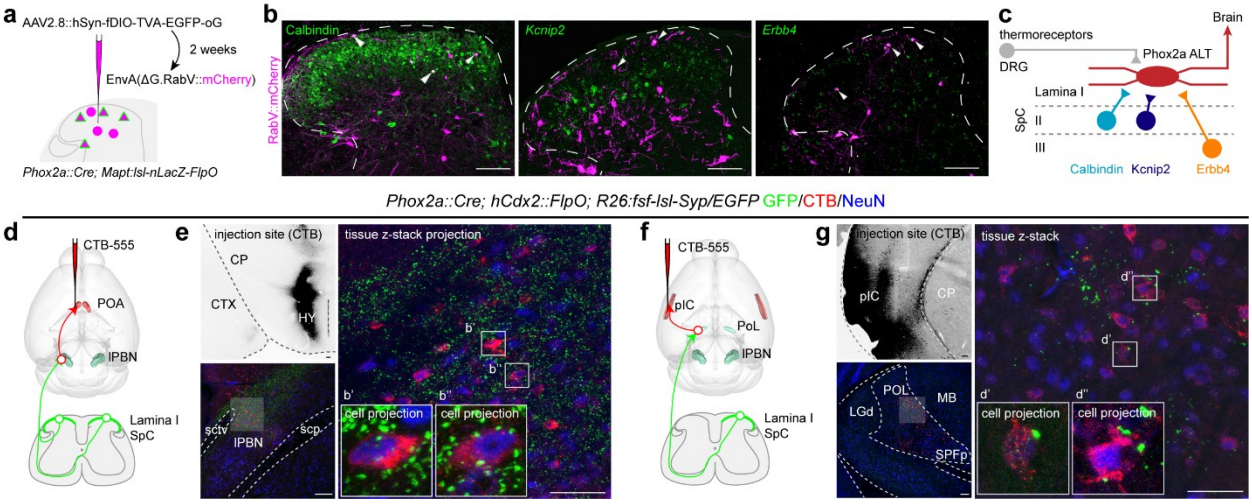

Fig. 4 | Situating Phox2a ALT neurons in thermosensory circuits. a, Monosynaptic rabies tracing experiment via infection with a helper virus and subsequent pseudotyped rabies injected into the lumbar spinal cord. **b,** Rabies-infected spinal dorsal horn neurons (magenta) expressing Calbindin protein, *Kcnip2* and *Erbb4* mRNAs (green). **c,** Summary of identified circuit ofPhox2a^{LamI} neurons. **d,** Experimental design of CTB injection into POA to retrogradely label cell bodies of PBN-POA projection neurons (red) and transgenic expression of EGFP in spinal Phox2a ALT termini (green) in *Phox2a::Cre; hCdx2::FlpO; R26:fsf-lsl-Syn/EGFP* mice. **e,** Axon termini of Phox2a ALT neurons in the lPBN (GFP, green) are juxtaposed on lPBN-POA projecting neuron somata (CTB, red). **f,** Experimental design of CTB labelling of PoL-pIC projections as in **(d)**. **g,** Axon termini in the PoT (GFP, green), on somata of thalamocortical projecting neurons (CTB, red). Abbreviations: CTX (cortex), CP (caudoputamen), HY (hypothalamus), lPBN (lateral parabrachial nucleus), scp (superior cerebellar peduncles), sctv (ventral spinocerebellar tract), pIC (posterior insular cortex), CP (caudoputamen)LGd (dorsal lateral geniculate complex), MB (midbrain), PoL (posterior limiting nucleus of the thalamus), SPFp (subparafascicular nucleus, parvicellular part). Scale bar: 100 μm in **(b, e & g left)** and 50 μm in **(e & g right)**.

449

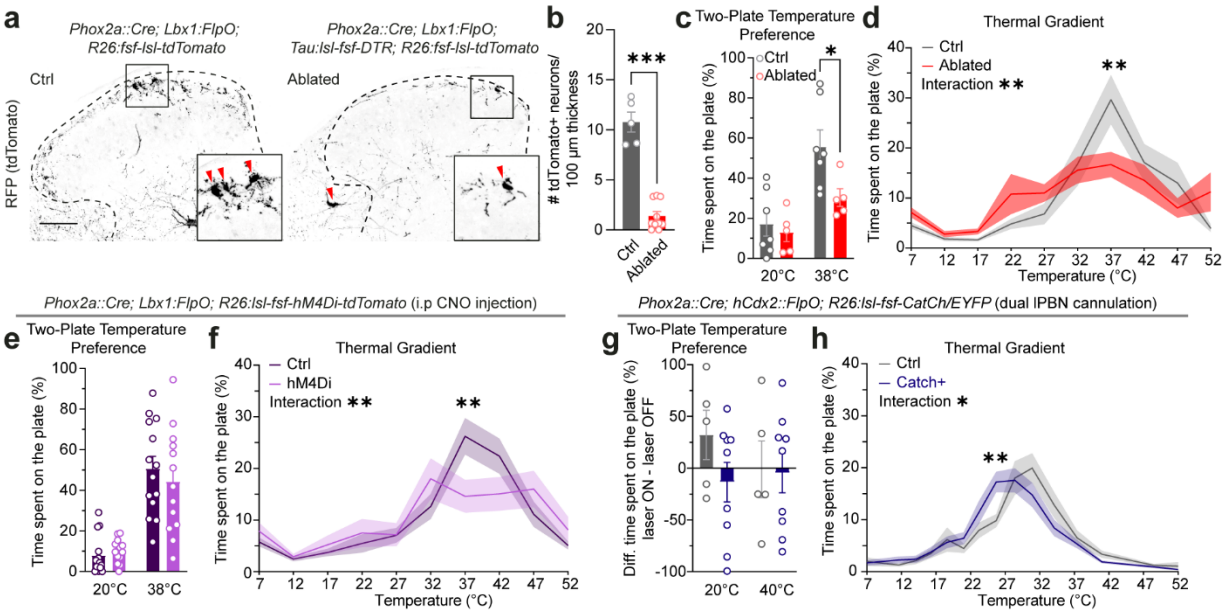

450

451 **Fig. 5 | Phox2a ALT neuron function in thermal preference. a,** Ablation of spinal Phox2a
452 neurons: transverse sections of the lumbar spinal cord from control (Ctrl) or ablated mice showing
453 tdTomato-positive *Phox2a::Cre; Lbx1:FlpO* neurons. **b,** Quantification of tdTomato+ cells in the
454 lumbar spinal cord co-expressing NeuN in control and ablated mice. Cell numbers are averaged
455 per 100 µm thickness (4 sections of 25µm thickness). **c, d,** Behavioural assessments in the control
456 and ablated mice in two-plate temperature preference assay, between 30°C vs. 20°C, or 30°C vs.
457 38°C **(c)**, and a temperature gradient ranging from 7°C to 52°C and divided into zones of 5°C **(d)**.
458 **e-h,** Behavioural assessments of control and mice with Phox2a ALT neurons being
459 chemogenetically inactivated (hM4Di; **e, f**) or optogenetically activated **(g, h).** Two-plate
460 temperature preference test **(e, g)** was performed as in **(c)** except for difference of percentage of
461 time on the plate was calculated between laser on and laser off in **(g)**. Thermal gradient test **(f, h)**
462 as in **(d).** Scale bar: 100 µm in **(a)**. Mean ± SEM. *p <0.05, **p <0.01, ***p < 0.001, non-

significant not labelled. Ordinary Two-way Anova with Bonferroni's multiple comparisons test in **(c-h)**.

467 **Methods**

468 **Mouse line generation**

469 All procedures were approved by local committees, including the IRCM and Université Laval
470 Animal Care Committee, using Canadian Council for Animal Care (CCAC) regulations, and the
471 Ethical Review Process Applications Panel of the University of Glasgow, according to the UK
472 Animals (Scientific Procedures) Act 1986 and ARRIVE guidelines. Adult male and female mice
473 (6-19 weeks of age) were used, and sex ratio for all experiments was kept close to 1:1. Mice were
474 housed with a 12-hour: 12-hour light: dark cycle (light: 6h00 to 18h00) with food and water *ad*
475 *libitum*. Mice were maintained on a mixed 129/Sv and C57BL/6J, or pure C57BL/6J background
476 as indicated in the key resource table. In the ablation, chemogenetic activation, chemogenetic
477 inactivation, and optogenetic behavioural experiments, mouse lines containing *Phox2aCre/+* and
478 *Lbx1FlpO/+* or *hCdx2FlpO/+* was first generated[35,51], and bred with parents containing *Tau:DS-*
479 *DTR-/-, Ai65-/-* (ablation), or *Rosa:DS hM3Dq-mCherry-/-* (chemogenetic activation), or
480 Rosa:DS-hM4Di-tdTomato-/- (chemogenetic inactivation), or *Rosa:DS-CatCh-/-* (optogenetic) to
481 generate experimental mice (Phox2a^{abl}, Phox2a^{hM3Dq}, Phox2a^{hm4Di}, or Phox2a^{CatCh}) that carry all
482 transgenes, and littermate control mice that lack either *Phox2aCre* or *Lbx1FlpO* transgenes. For
483 detailed information of mouse strains used, see Supplementary Table 2.

484

485 **Immunohistochemistry**

486 Tissue dissection was as previously described[11,52]. For adult tissue collection, mice were first
487 anesthetized and transcardially perfused with 1xPBS solution followed by 4% PFA. Brains,spinal

488 cords and DRGs were collected and post-fixed overnight in 4% PFA on a shaker at 4°C, followed
489 by overnight wash in 1x PBS, and transfer to 30% sucrose until sunk. For embryonic tissue
490 collection, vaginal plugs were checked daily at 6h00, and the day of plug detection was noted as
491 embryonic day 0.5 (E0.5). On the day of E16.5, mothers were anesthetised with isoflurane and
492 received a cervical dislocation. Embryos were dissected in 1xPBS and followed by the same
493 fixation procedure as described above. Tissue was embedded in O.C.T. and stored at -80°C until
494 cryosectioning mounting on Superfrost plus slides which were dried and stored at -80°C until
495 processed for immunofluorescent protein or mRNA detection. For the former, slides were
496 rehydrated and washed in 1xPBS, and blocked with blocking solution (5% Normal Donkey Serum
497 (NDS) in 1xPBST (0.1% Triton X-100 in 1xPBS)) for 30 minutes at room temperature (RT).
498 Primary antibodies were added in 1% NDS blocking solution and coverslipped to incubate
499 overnight at 4°C. Slides were then washed with 1xPBS, and the secondary antibodies in 1xPBST
500 solution was applied for 2 hours at RT. Finally, the slides were washed in 1xPBS, mounted with
501 Mowiol, and imaged upon dried. For all detailed reagents used, see Supplementary Table 2.

502

503 ***In situ* mRNA localisation**

504 Cryosectioned slides were processed using RNAscope Multiplex Fluorescent v2 kits as per
505 manufacturer's protocol (https://acdbio.com/manual-assays-rnascope). For some Figure 1 and
506 Figure S1 experiments indicated in figure legends, immunohistochemical protein detection was
507 performed as above following mRNA detection and prior to the mounting.

508

509 **Stereotaxic surgery**

510 Mice received 1 mg/kg of body weight of buprenorphine intraperitoneal (i.p.) the day of the surgery.
511 During the surgery, mice were anesthetised with 4% isoflurane (induction phase) followed by 2%
512 isoflurane (maintenance phase) in a mixture of 70% N_2 and 30% O_2, and placed in a stereotaxic
513 apparatus. Following shaving, the skin was disinfected with iodine and ethanol. Intracranial and
514 intraspinal injections were performed generally as previously described[11,53]. For all intracranial
515 injections, the following coordinates (in mm) and volumes for single injection of CTB were used:
516 5.0 AP, ±1.5 ML, 2.75 DV, 250 nL for PBN, 0.5 AP, -4.25 ML, 3.0 DV, 300 nL for pIC, 0.1 AP, -
517 0.3 ML, 5.8 DV, 300 nL for POA, similar to those previously described[11]. For intraspinal injections,
518 mice were anesthetised as above, and the intervertebral space between T13 and L1 of vertebral
519 bones (L3-L4 lumbar spinal cord) was exposed. Three injections of 333 nL AAVs or rabies viruses
520 were made along the AP axis (spaced 400 µm apart along the AP axis, 0.48 ML, 0.26 DV)[54]. All
521 injections were performed at a rate of 100 nL/minute, and the glass capillary was held for another
522 3 minutes after the injection to prevent leakage. Mice recovered in a heated chamber until
523 ambulatory before returning to their home cages.

524

525 **Patch-clamp recording in semi-intact preparation**

526 Semi-intact preparation was performed largely as previously described[19,30]. Briefly, adult mice
527 were perfused with oxygenated (95% O_2/5% CO_2) sucrose-based artificial cerebrospinal fluid
528 (ACSF) (in mM; 3.0 KCl, 1.2 NaH_2PO_4, 0.5 $CaCl_2$, 7.0 $MgCl_2$, 26.0 $NaHCO_3$, 15.0 glucose, 251.6
529 sucrose, 1.0 Na ascorbate, and 1.0 Na pyruvate) at room temperature. Immediately after perfusion,

530 the spinal cord (~C2-S6) and the right hindlimb were excised and submerged in sucrose-based
531 ACSF circulated at 5 mL/min in a Sylgard-lined dish. Next, the saphenous nerve and the femoral
532 cutaneous nerve and the innervated skin were dissected, and the L2 and L3 dorsal root ganglion
533 were kept on the spinal cord. Dural and pial membranes were carefully removed and spinal cord
534 was pinned onto the Sylgard block with the right dorsal horn facing upward. The chamber was
535 then transferred to the rig and rinsed with normal ACSF solution (in mM; 125.8 NaCl, 3.0 KCl,
536 1.2 NaH_2PO_4, 2.4 $CaCl_2$, 1.3 $MgCl_2$, 26.0 $NaHCO_3$, and 15.0 glucose) saturated with 95% O2/5%
537 CO2 at 25˚C for at least 15 minutes. Patch-clamp recordings were performed up to 4 hours after
538 dissection. Neurons were first visualized with a fixed-stage upright microscope and a narrow-beam
539 infrared LED as described previously. Whole-cell patch-clamp recordings were made with a
540 pipette constructed from thin walled single-filamented borosilicate glass with resistances of 6 -12
541 MΩ. Electrodes were filled with an intracellular solution (in mM; 130.0 K gluconate, 10.0 KCl,
542 2.0 $MgCl_2$, 10.0 HEPES, 0.5 EGTA, 2.0 ATP-Na, 0.5 GTP-Na, and 0.2% Neurobiotin, pH adjusted
543 to 7.3 with 1.0 M KOH). Neurobiotin (Vector Labs Peterborough, UK) was added to confirm
544 recording from the target cell. Signals were acquired with an amplifier (Axopatch 200B; Molecular
545 Devices, Sunnyvale, CA). The data were low-pass filtered at 2 kHz and digitized at 10 kHz with
546 an A/D converter (Digidata 1550B; Molecular Devices) and stored using a data acquisition
547 program (Clampex version 11; Molecular Devices). The liquid junction potential was not corrected.
548 Mechanical stimulation was applied using a 4.0 g von Frey filament. Thermal stimulation was
549 applied using hot (50˚C) and cold (15˚C) saline applied gently to the skin using an eye dropper.

550

551 **Morphological analysis**

552 Neurobiotin-labelled cells from electrophysiological recordings were revealed by incubating in
553 avidin-Alexa 555 (1:1000; Jackson ImmunoResearch) in 1xPBS containing 0.3% Triton X-100.
554 They were imaged with a confocal microscope through a 63× oil-immersion lens (numerical
555 aperture 1.4) at 0.5-µm z-spacing with all visible and distinguishable axonal and dendritic arbors.
556 Morphometric data for dendritic trees of all the reconstructed cells were obtained from
557 Neurolucida Explorer. The dendritic parameters were extracted as described previously[55]. To make
558 an objective comparison between the cool-selective and non-cool selective neurons, we performed
559 cluster analysis using Ward's method as described previously[55,56]. To reduce the dimensionality of
560 the original data while preserving variance, we calculated principal components from the data set.
561 The number of principal components to be retained for cluster analysis was then determined from
562 a screen test.

563

564 ***In vivo* calcium imaging**

565 *In vivo* Ca2+ imaging in *Phox2a::Cre; R26:lsl-GCamP6s* mice was performed largely as described
566 previously[23]. Briefly, animals were anesthetised with 100 mg ketamine, 15 mg xylazine, and 2.5
567 mg acepromazine per kg of body weight in saline, and then received a lumbar laminectomy and
568 were fixed on a spinal stabilizing apparatus. L3-L4 region was imaged with a two-photon
569 microscope using a 940 nm tunable femtosecond laser. RAW image sequences were acquired at
570 1000 x 500 pixels at a rate of 32Hz and with a pixel size of 0.385 µm. During the imaging, the
571 plantar side of the hind paw of the animal was stimulated by repeated manual brushing with a
572 paintbrush, pinching with serrated forceps, or thermal stimuli delivered by a feedback-controlled
573 Peltier device and a 1 x 1 cm thermal probe (TSA-II-NeuroSensory Analyzer, Medoc). Each

574 stimulus was provided with at least 3-5 minutes intervals and started with innocuous brush and
575 thermal stimuli, then noxious pinch to prevent sensitization. After acquisition, RAW image
576 sequences were converted into TIFF format in ImageJ and registered with a custom-built
577 MATLAB (MathWorks) function through rigid body translation alignment based on the 2D cross-
578 correlation to correct for movement. Background pixel value was defined by the average pixel
579 value of a region of interest (ROI) containing no visible neurons. Neuronal ROIs were drawn
580 manually in the cytoplasm of visible neurons. The average fluorescence intensity of a given ROI
581 was defined as Ft, calculate as the mean pixel intensity within that neuronal ROI minus that of the
582 background ROI. Ca2+ amplitude was defined as $\Delta F/F0 = (Ft-F0)/F0$, where F0 is the baseline
583 fluorescence value, measured as the average of the first two seconds of Ft. Positive responses were
584 detected and measured automatically using a custom tool written in Spike2 (Cambridge Electronic
585 Design [CED]) and confirmed by visual inspection, and all data were exported into Microsoft
586 Excel Table for subsequent statistical analysis[23,57].

587

588 **Behavioural assays**

589 The experimenters were blinded to genotypes during the experiment and video analysis. Prior to
590 all tests, mice were habituated to the behaviour test room for at least 30 minutes in their home
591 cages except for von Frey and acetone test when mice were habituated in the test chambers, and
592 test chambers and apparatus were always cleaned and deodorized with Peroxygard between
593 animals. Behaviour tests except vF were filmed for post hoc analysis. All tests were performed on
594 separate days to prevent sensitization or adaptation.

The **thermogradient test** was performed using Thermal Gradient Test 2.0 (Bioseb)[58]. In brief, a 120 cm metal corridor was set at a continuous and stable temperature gradient from 7°C to 52°C, and its orientation was randomized. Ten virtual temperature zones with a 5°C-step difference at the centre were defined for two lanes for two mice for each test. Mice were introduced in the middle of the corridor and allowed to explore freely for 30 minutes, and their position was recorded by an overhead camera for video tracking. The percentage of cumulative time spent in each temperature zone was reported for the second half of the test.

The **two-plate temperature preference test** was performed with Thermal Place Preference-Two Temperatures Choice Nociception Test (Bioseb)[58]. Mice were allowed to explore the two compartments of the metal plate set at experimental temperatures (38°C or 20°C) and neutral temperatures (30°C) for 10 minutes with overhead camera recording for video tracking. Mice were first tested for their preference with both plates set at 30°C (Day 1), and those exhibited high spatial preference (>75% of one compartment) were excluded from the analysis. Mice were then tested for their preference of the experimental temperature on Day 2 and Day 3, with the sequence of the temperature and its compartment randomized.

For the **von Frey test**, mice were placed in a plexiglass chamber (4 × 2.2 × 2.5 cm each) with metal dividers on a mesh floor. A set of nylon von Frey filaments (0.008, 0.02, 0.04, 0.07, 0.16, 0.4, 0.6, 1.0, 1.4 g) were used to stimulate the plantar surface of the mouse hind paw, using the "up-down" method of Dixon, and withdraw threshold was calculated accordingly, ranging from 0 (most sensitive) to 2 (least sensitive)[59].. The filaments were calibrated every time prior to the test.

616 The **foot clip test** was performed as performed as described previously[60]. Briefly, mice
617 were pinched on the hindpaw with a toothless mechanical clip and then placed into a plexiglass
618 cylinder on a plexiglass sheet and video recorded from below for 60 seconds. The total amount of
619 time licking the clipped paw was recorded.

620 For the **hot plate and cold plate test**, mice were placed in the hot-cold plate apparatus (4”
621 x 8”, IITC PE34) at set temperature of 53°C ± 0.1°C (hot plate) or 1°C ± 0.1°C (cold plate), and
622 video recorded from front-above with a mirror at the back of the chamber to provide clear view of
623 both sides of the mice[11,61]. For the hot plate, mice were removed once licking of both hind paws
624 were observed, or cutoff at 15 seconds. For the cold plate, mice were recorded for 60 seconds. The
625 latency of withdraw of both paws were recorded immediately during the test, and the videos were
626 further analysed to record the latency to lick the hind paws. Scores were arbitrarily assigned to the
627 cold plate test as the following: 0 – no reaction, 1 – tiptoeing or avoidance, 2 – withdrawal or
628 flinching, 3 – licking.

629 For the **acetone test**[11,62] mice were placed in a plexiglass chamber (4 × 2.2 × 2.5 cm each)
630 with metal dividers on a mesh floor. A drop of acetone extruded from the blunt end of a 5ml syringe
631 was applied to either hind paw of the mouse. Mice were stimulated 5 times in total, with an inter-
632 trial-interval of 5 minutes, and each trial was recorded for 60 seconds following the stimulation.
633 The videos were analysed with BORIS and the total licking time was reported as a sum of 5 trials[63].

634 For the **capsaicin test**[11,61], 20 μL capsaicin solution (1.5 ug/20 ul in 1xPBS) at RT was
635 injected intraplantarly in the hind paw using a standard 28G insulin syringe (BD). Mice were
636 placed in a plexiglass cylinder with blocked visual to other mice. The video was recorded for 15
637 minutes and then analysed for the duration of licking behaviour.

638 For **the open field test**, mice were placed in a square chamber (50 x 50 x 40 cm) and
639 allowed to freely explore for 30 minutes[64]. An overhead tracking camera recorded their movement
640 in the chamber and the cumulative distance they travelled was reported.

641

642 **Optogenetic Stimulation**

643 Animals were implanted with optical fibers (NA 0.22, 200 μm core, Doric) over the lateral
644 parabrachial nucleus (AP: -5.20, ML: ±1.40, DV: -2.50, based on The Mouse Brain in Stereotaxic
645 coordinates, 2nd edition, ISBN 0-12-547636-1, Paxinos & Franklin[65]). The laser intensity was
646 10mW on each side of 488 nm light (20 Hz, 5 ms-duration pulses). Mice were habituated to the
647 cables prior to behavioural tests.

648

649 **Quantification and statistical analysis**

650 Confocal images of cells are processed with ImageJ software and are quantified with its cell
651 counter plugin. Video recordings of mice behaviours are quantified using Behavioral Observation
652 Research Interactive Software (BORIS) and annotated frame based. Data was recorded and sorted
653 in Microsoft Excel and imported in GraphPad Prism software for statistical analysis and display.
654 Significance is represented as ns: nonsignificant, *$p < 0.05$, **$p < 0.01$ or ***$p < 0.001$ for all
655 figures.

656

657 **Data availability**

658 All other data are available in the main paper and supplementary materials. All materials are
659 available through requests to the corresponding author.

660

661 **Acknowledgements**

662 We thank the Goulding lab for sharing the following mouse lines with us: *hCdx2::FlpO;*
663 *Rosa26:ds-HTB; Lbx1::FlpO; Tau:ds-DTR*, Dr. Mark Hoon for sharing *Trpm8:Flp* mice, Dr.
664 Marie-Eve Paquet and her team for developing all the AAVs and Rabies viruses used in this project
665 (Viral Vector Core of Canadian Neurophotonics Platform), Dr. Magali Millecamps (ABC Platform,
666 McGill Univeristy) for contributing to the thermogradient, two-plate temperature preference, light
667 brush, and hot/cold plate tests, Meirong Liang for genotyping. This work was supported by project
668 grants from the Canadian Institutes of Health Research (CIHR; CIHR; PJT-162225, MOP-77556,
669 PJT-153053, PJT-159839, and PJT-197987) to A.K., Natural Science and Engineering Research
670 Council Discovery grant CG139292 to F. W., and the Medical Research Council (MR/V033638/1)
671 to J.H. and A.J.T. A.K. held the Doggone Foundation Chair of Excellence in Pain and received
672 support from the Foundation IRCM. X.Z. is a recipient of a Fonds de recherche du Québec -Santé
673 doctoral scholarship. We thank Drs. Allan Basbaum, Brian Roome, Bo Duan, Ran Chen, and
674 Sebastian Choi for their generous feedback on the manuscript and the project.

675

676 **Author contributions**

X. Z. Performed all experiments except for the electrophysiology, calcium imaging and partial behavioural experiments as described in Methods, and analysed the data. Partial behavioural experiments were performed by M.M and S.F., and analyzed by X.Z. F.W. performed the calcium imaging experiments. A.M., M.K., and J.H. performed the electrophysiological experiments, and K.A.B. and A.M. performed subsequent morphological analyses, M. E. P. provided key reagents, A.K., Y.d.K., J. H. and A.J.T. supervised the study and acquired funding. A.K. and X.Z. wrote the manuscript.

Competing interests: Authors declare that they have no competing interests.

686 **Extended Data**

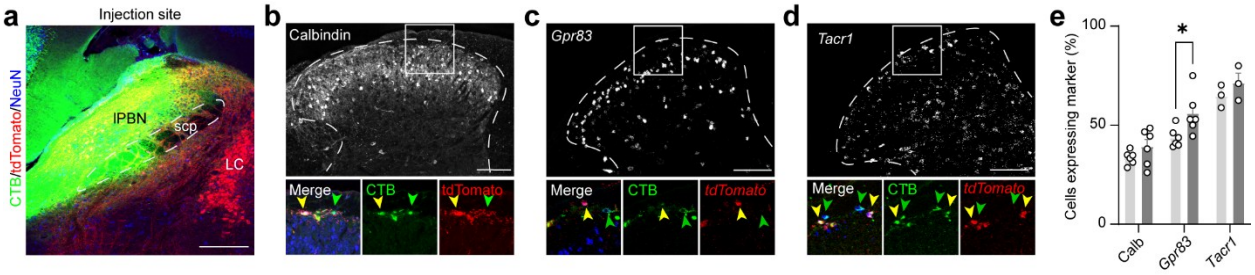

687

688 **Extended Data Fig. 1 | Additional characterisation of lumbar Phox2a ALT neurons. a,**
689 Representative images of the injection site in the lateral parabrachial nucleus (lPBN). **b-d,**
690 Additional staining of CTB (green), tdTomato (red), and Calbindin antibody (white, **b**) or
691 RNAscope probes targeting tdTomato (red) and Gpr83 **(c)** or Tacr1 mRNA (white, **d**) in Phox2a+
692 (yellow arrowhead) or Phox2a- (green arrowhead) ALT neurons. **e,** Quantification of the
693 percentage of Phox2a+ (light gray) or Phox2a- (dark gray) ALT neurons co-expressing the marker.
694 Scale bar: 100 µm in **(a-d)**. *p <0.05, **p <0.01, ***p < 0.001, non-significant not reported. Mann-
695 Whitney test in **(e)**.

696

697

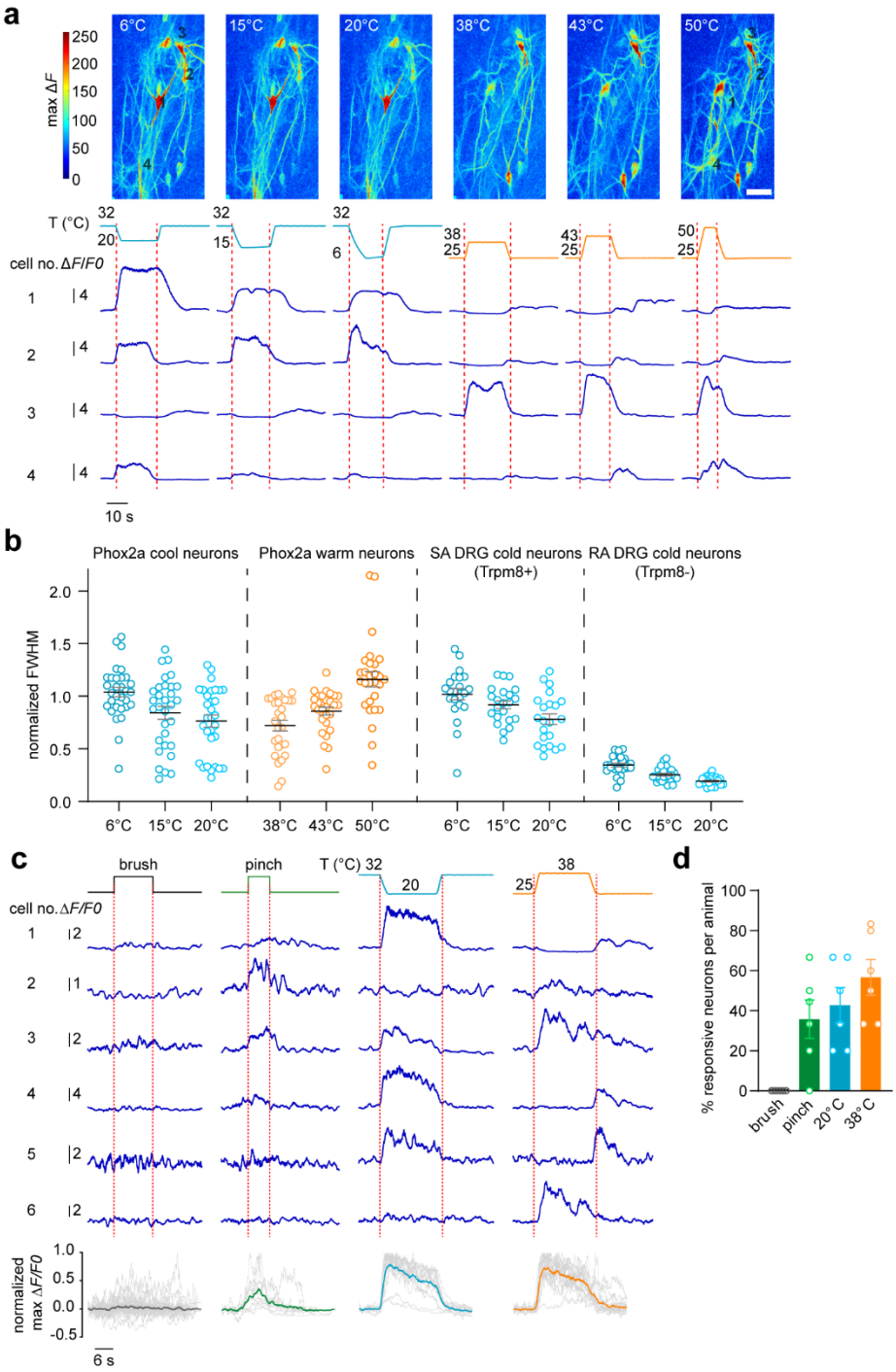

698

699 **Extended Data Fig. 2 | Phox2a lamina I ALT neurons are tuned to temperature changes. a,**

700 Representative imaging window and calcium curves from four neurons showing typical responses

701 to thermal stimuli as in Figure 1 (**h**), cell number same as the row number. Cell number 1 and 2

are typical cool-selective Phox2a neurons, cell number 3 is a typical warm-selective Phox2a neuron, and cell number 4 is a cold-heat responding Phox2a neuron. **b,** Normalized full-width-half-maximum (FWHM) of calcium responses over thermal stimulation duration in Phox2a cool-selective or warm-selective neurons showing a slow adaptive (SA) characteristic similar to SA cool (Trpm8+) thermoreceptors but distinct from rapid adaptive (RA) cool thermoreceptors. **c, Top:** representative calcium curves from six neurons in response to manual brush, manual pinch, or thermal stimuli as in Fig. 1 **(h)**. Bottom: individual calcium traces and the population average from all neurons tested. **d,** Summary of the percentage of neurons responded to each stimulus within each animal (N=6).

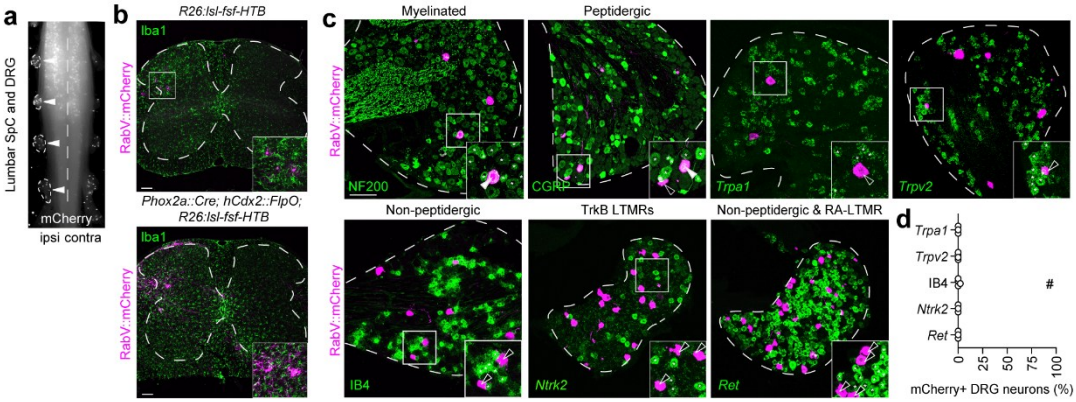

712

713 **Extended Data Fig. 3 | Sensory neuron inputs to Phox2a ALT neurons. a,** Representative image
714 of whole-mount lumbar spinal cord with DRGs attached containing rabies infected cell expressing
715 mCherry (white). **b,** Representative images showing that control animals with no Cre and FlpO
716 (TVA-) were not infected by rabies in neurons, but rabies infected microglia in both TVA- and
717 TVA+ animals. **c,** Representative images of rabies-infected neurons not co-expressing Ntrk2, Ret,
718 Trpv2 mRNA or IB4 protein. **d,** Quantification of the percentage of rabies infected DRG neurons
719 co-expressing the markers over all rabies infected cells (mCherry+ DRG neurons). #: rabies-
720 resistant non-peptidergic neurons expressing IB4. **e,** Cell body sizes of all rabies-infected DRG
721 neurons. Both small, median, and large diameter neurons were found., but the majority are small
722 to median size. Each curve represents an individual animal, N=5. Scale bar: 100μm in **(b, c)**.

723

724

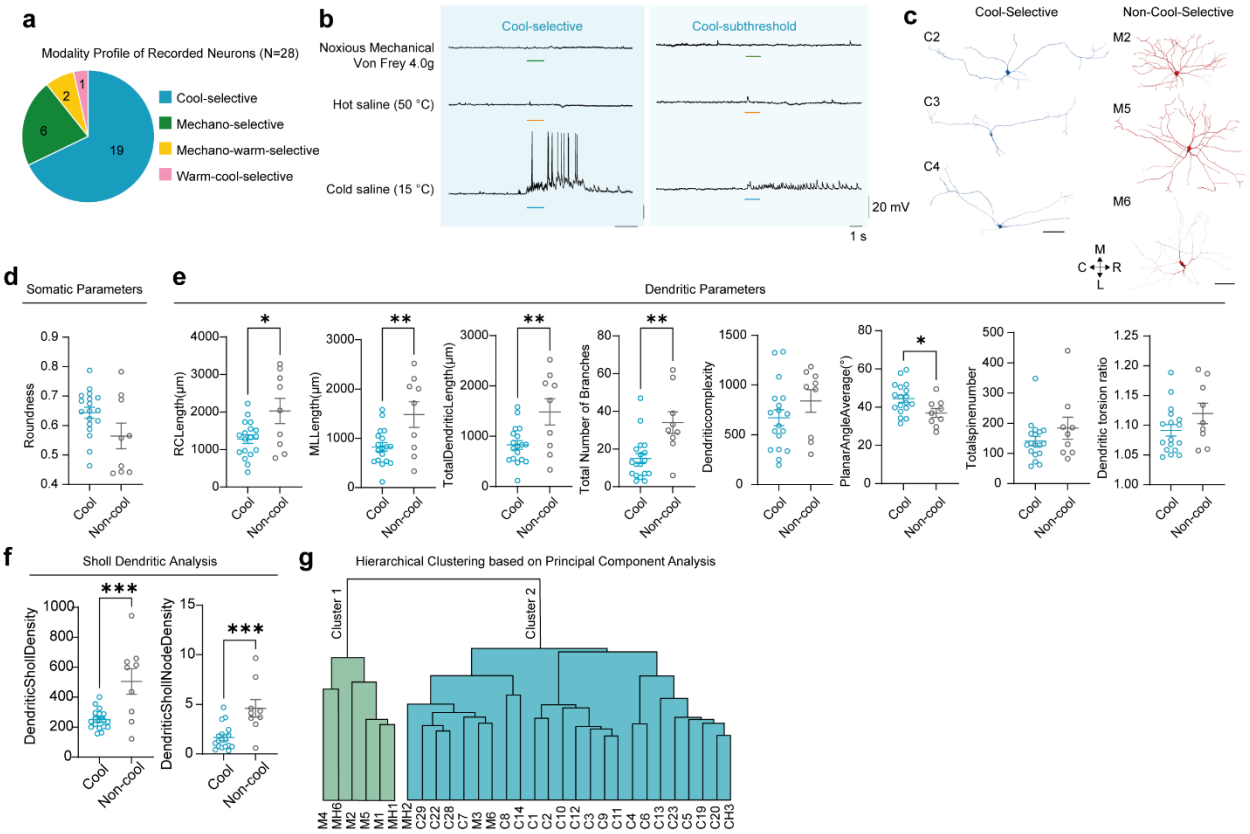

725

726 **Figure S4 | Further physiological and morphological characterization of Phox2a^{LamI} ALT**
727 **neurons. a,** Pie chart of the response profile to all modalities of stimuli of all Phox2a^{lamI} neurons
728 recorded (N=28). **b,** Representative traces of cool-selective and cool-subthreshold Phox2a^{lamI} cells
729 with Trpm8 fibre contact, similar as described in **(Fig. 3e)**. **c,** Additional reconstructed cells of
730 cool-selective and non-cool selective Phox2a^{lamI} neurons. **d-f,** Other somatic and dendritic
731 parameters of cool-selective and non-cool selective Phox2a^{lamI} neurons. **g,** Two major clusters
732 identified by hierarchical clustering based on the principal component analysis of the
733 morphological parameters from neurobiotin-filled cells. C: cool-selective, M: mechano-selective,
734 MH: mechano-warm-selective, CH: warm-cool-selective. *p <0.05, **p <0.01, ***p < 0.001, non-
735 significant not reported. Mann-Whitney test in **(d-f)**.

736

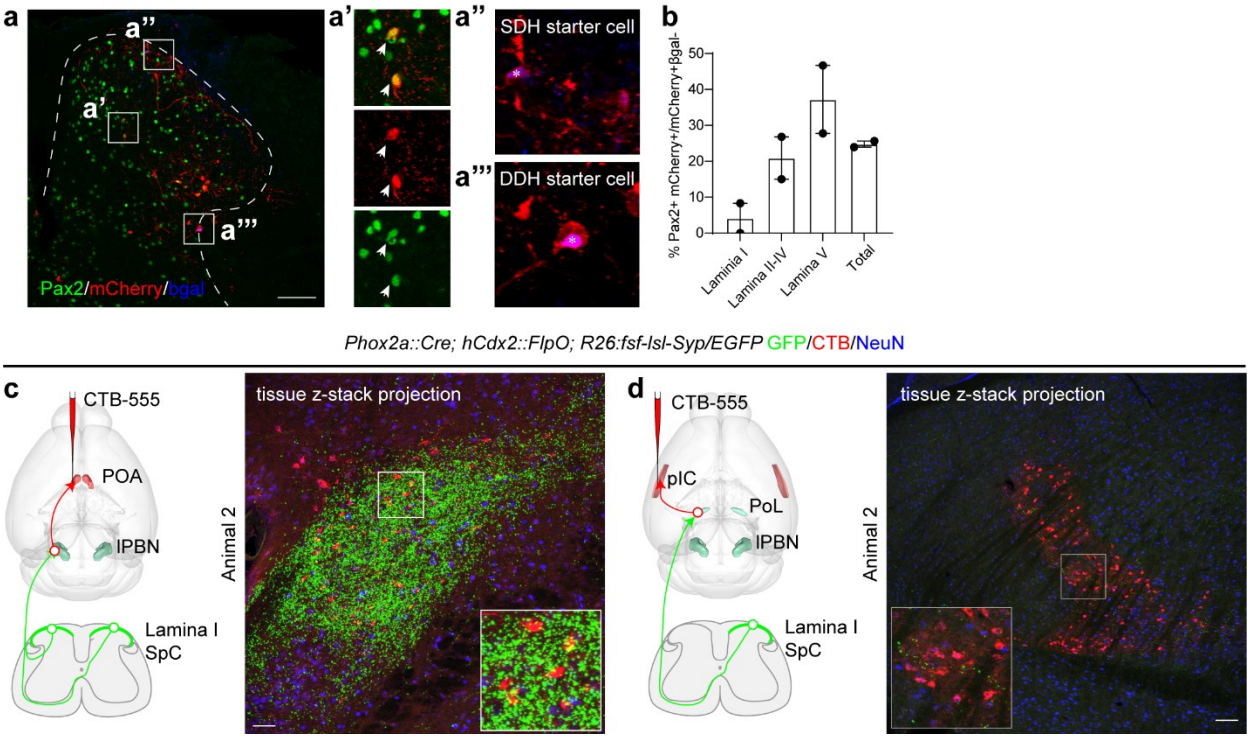

Extended Data Fig. 5 | Additional characterization of Phox2a neurons in local and supraspinal circuits. a, Representative picture of local spinal dorsal horn infected with rabies (mCherry, red) and labeling of the inhibitory neuron marker Pax2 (green). Starter cell revealed by β-galactosidase expression (blue, **a''** and **a'''**). **b,** Percentage of interneurons presynaptic to Phox2a neurons that are inhibitory (Pax2+), shown by laminar distribution. **c,** Additional animal showing Phox2a axon terminals on lPBN-POA projecting neurons, observed in total N=5 animals with similar pattern**. d,** Additional animal showing Phox2a axon terminals on PoL-pIC projecting neurons, observed in total N=3 animals with similar pattern. Scale bar 100 μm in all.

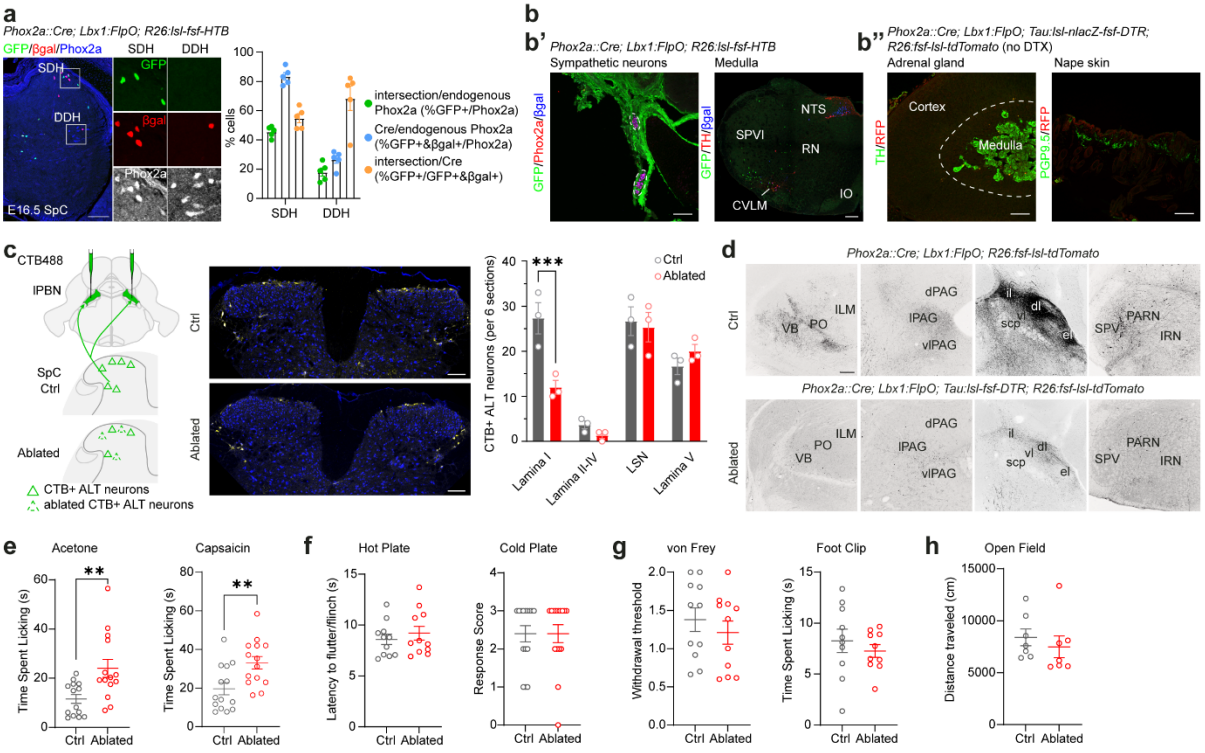

Extended Data Fig. 6 | Characterization of the ablation model and nocifensive and locomotor behaviours. a, Intersectional efficiency of *Phox2a::Cre* alone or with *Lbx1:FlpO* in the superficial dorsal horn (SDH) and deep dorsal horn (DDH) in comparison to the endogenous Phox2a protein expression. β-galactosidease: Cre expression only; GFP: Cre and FlpO co-expression. **b,** *Phox2a::Cre; Lbx1:FlpO* intersection does not target cells in the sympathetic ganglion, noradrenergic (TH+) medullary areas, adrenal gland, or skin at the nape area. **c,** Representative pictures showing that the ablation mainly decreased the number of lamina I but not deep laminae ALT neurons (CTB, green). **d,** Ablated animals showed loss of innervation in many brain areas that normally receive abundant Phox2a ALT innervations as in control (ctrl). **e-h,** Licking responses to acetone and capsaicin application were increased in Ablated group **(e)**. Reflexive withdrawal in response to hot and cold plate **(f)**, as well as to von Frey filaments stimulation (g), licking responses to mechanical stimuli **(g)**, and general locomotion **(h)** did not differ between

759 Ablated and control animals. Scale bar: 100 μm in **(a, b', c)**; 200 μm in **(b'', d)**. Mean ± SEM. *

760 $p<0.05$, ** $p<0.01$, *** $p<0.001$. Mann-Whitney test **(e-g)**.

761

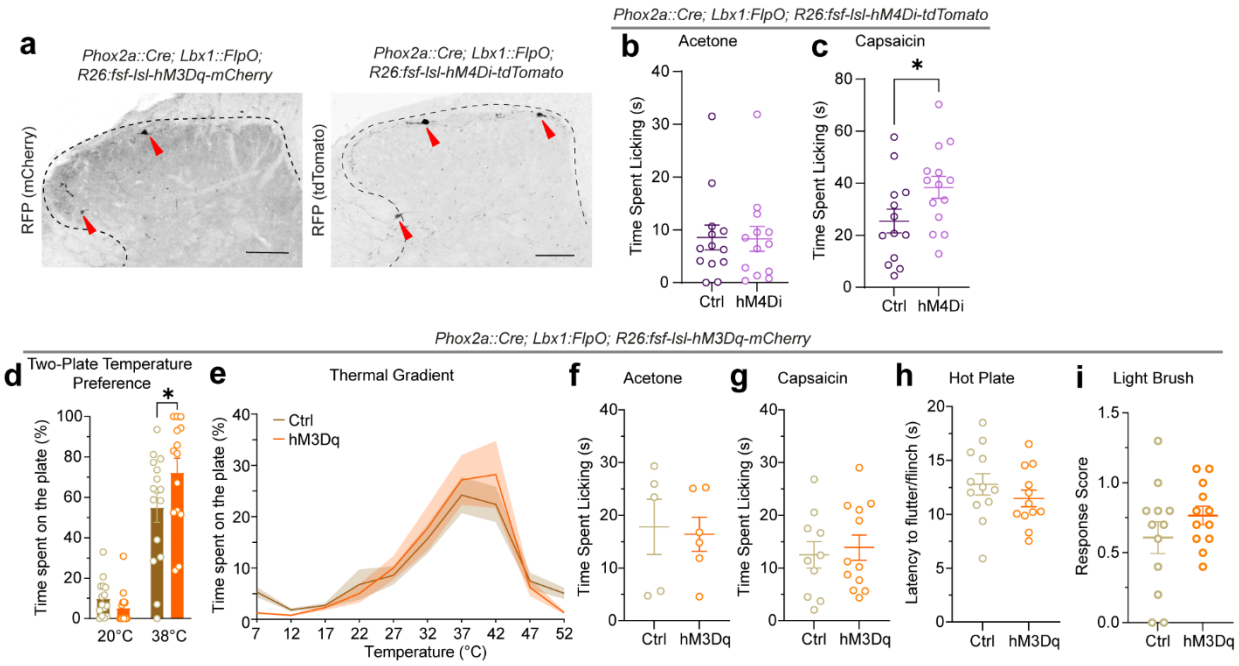

762

763 **Extended Data Fig. 7 | Characterization of chemogenetic models and their behaviours. a,**
764 Expression of DREADDs (hM3Dq and hM4Di) in the *Phox2a::Cre; Lbx1:FlpO* intersected
765 Phox2a ALT neurons (red arrow). **b, c,** Chemogenetic inhibition did not alter licking response to
766 acetone **(b)** but increased licking following intraplanter injection of capsaicin **(c). d, e,**
767 Chemogenetic activation did not affect behavior in a the two-plate temperature preference at 20°C
768 **(d)** or thermal gradient **(e)** assays. **f-i,** Chemogenetic activation did not alter response to acetone
769 **(f)**, intraplanter injection of capsaicin **(g)**, hot plate **(h)**, or light brush **(i).** Mean ± SEM. * $p<0.05$,
770 ** $p<0.01$, *** $p<0.001$. Mann-Whitney test **(b, c, f-i)**. Two-way ANOVA with Bonferroni's
771 multiple comparisons **(d, e)**.

772

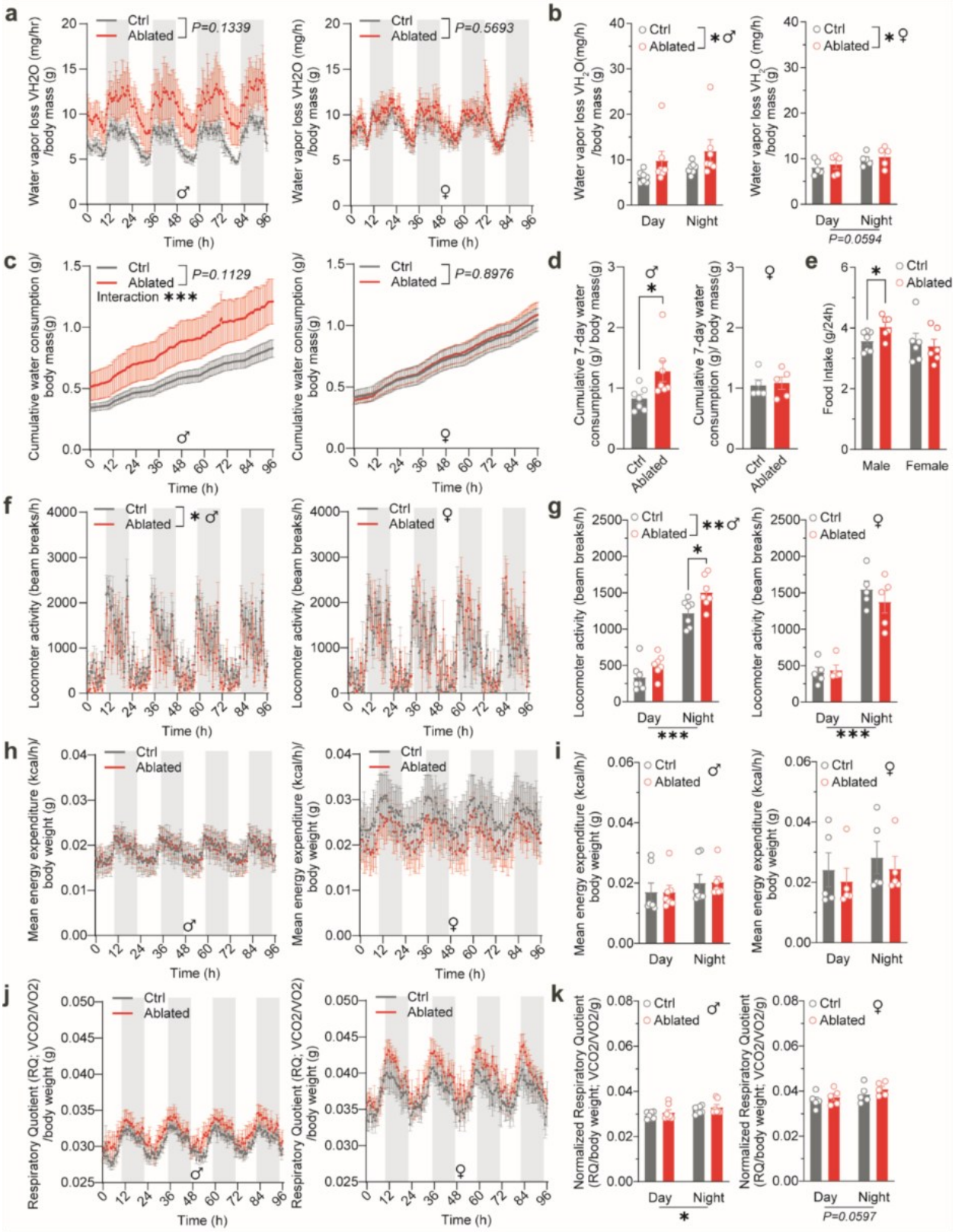
a
Ctrl
Ablated
P=0.1339
Water vapor loss VH2O (mg/hr) /body mass (g)
Time (h)
P=0.5693
b
Water vapor loss VH2O(mg/h) /body mass (g)
Day
Night
P=0.0594
c
P=0.1129
Interaction ***
Cumulative water consumption (g)/ body mass(g)
P=0.8976
d
Cumulative 7-day water consumption (g)/ body mass(g)
e
Food Intake (g/24h)
Male
Female
f
Locomoter activity (beam breaks/h)
g
h
Mean energy expenditure (kcal/h)/ body weight (g)
i
j
Respiratory Quotient (RQ; VCO2/VO2) /body weight (g)
k
Normalized Respiratory Quotient (RQ/body weight; VCO2/VO2/g)
P=0.0597

773

774 **Extended Data Fig. 8 | Metabolic parameters of Ablated mcie were largely unaffected. a, b,**
775 Normalized water vapor loss (VH_2O) of males and females across a four-day time scale **(a)** and
776 averaged by daytime versus nighttime **(b)**. **c, d,** Normalized cumulative water consumption of
777 males and females across a four-day time scale **(c)** and the total weight of the last measurement
778 **(d)**. **e,** Averaged food intake per 24 hours of males and females. **f, g,** Hourly locomotor activity by
779 number of beam breaks of males and females across a four-day time scale **(f)** and averaged by
780 daytime versus nighttime **(g)**. **h, i,** Normalized energy expenditure of males and females across a
781 four-day time scale **(h)** and averaged by daytime versus nighttime **(i)**. **j, k,** Normalised respiratory
782 quotient (RQ) of males and females across a four-day time scale **(j)** and averaged by daytime
783 versus nighttime **(k)**. Mean ± SEM. * $p<0.05$, ** $p<0.01$, *** $p<0.001$. Two-way ANOVA
784 Repeated Measurement **(a, c, f, h, j)**. Ordinary Two-way ANOVA with Bonferroni's multiple
785 comparisons **(b, e, g, i, k)**. Mann-Whitney test **(d)**.

786

787

788

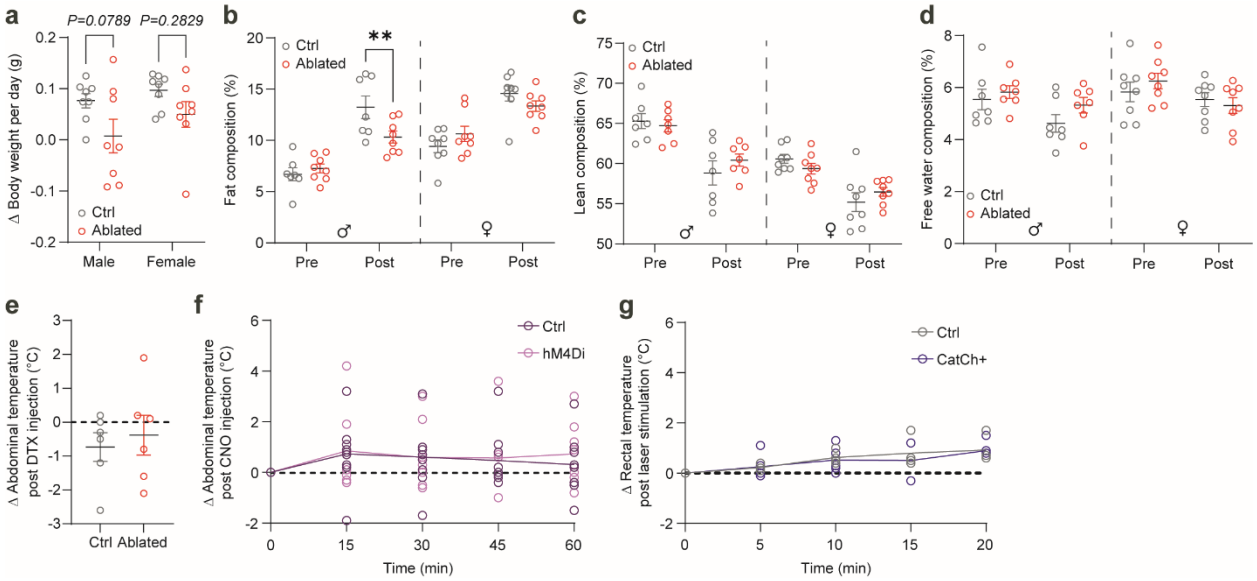

Extended Data Fig. 9 | Body composition and core temperature changes in Ablated and chemogenetic model mice. a, Averaged body weight changes per day of males and females. **b-d,** Body composition of fat **(b)**, lean **(c)**, and free water **(d)** of male and female mice pre- and 30 days post-injection of DTX. **e, f,** Core body temperatures changes measured by abdominal-implanted chips (UIDTM) 30 days post-injection of DTX **(e)**, 60 minutes post-injection of CNO **(f),** or measured by rectal probe every 5 minutes after optogenetic activation for 20 minutes **(g)**. Mean ± SEM. * $p<0.05$, ** $p<0.01$, *** $p<0.001$. Ordinary Two-way ANOVA with Bonferroni's multiple comparisons **(a)**, Mann-Whitney test **(e)**, Two-way ANOVA Repeated Measurement with Bonferroni's multiple comparisons **(b-d, f, g)**.

References

1 Wercberger, R. & Basbaum, A. I. Spinal cord projection neurons: a superficial, and also deep analysis. *Curr. Opin. Physiol.* **11**, 109-115 (2019). https://doi.org/10.1016/j.cophys.2019.10.002

2 Allard, J. Physiological properties of the lamina I spinoparabrachial neurons in the mouse. *J. Physiol.* **597**, 2097-2113 (2019). https://doi.org/10.1113/jp277447

3 Craig, A. D., Krout, K. & Andrew, D. Quantitative Response Characteristics of Thermoreceptive and Nociceptive Lamina I Spinothalamic Neurons in the Cat. *J. Neurophysiol.* **86**, 1459-1480 (2001). https://doi.org/10.1152/jn.2001.86.3.1459

4 Bester, H., Chapman, V., Besson, J. M. & Bernard, J. F. Physiological properties of the lamina I spinoparabrachial neurons in the rat. *J Neurophysiol* **83**, 2239-2259 (2000). https://doi.org/10.1152/jn.2000.83.4.2239

5 Yarmolinsky, D. A. *et al.* Differential modification of ascending spinal outputs in acute and chronic pain states. *Neuron* **113**, 1223-1239.e1225 (2025). https://doi.org/10.1016/j.neuron.2025.01.031

6 Chisholm, K. I. *et al.* Encoding of cutaneous stimuli by lamina I projection neurons. *PAIN* **162**, 2405-2417 (2021). https://doi.org/10.1097/j.pain.0000000000002226

7 Andrew, D. & Craig, A. D. Spinothalamic lamina I neurones selectively responsive to cutaneous warming in cats. *J. Physiol.* **537**, 489-495 (2001). https://doi.org/10.1111/j.1469-7793.2001.00489.x

8 Dostrovsky, J. O. & Craig, A. D. Cooling-specific spinothalamic neurons in the monkey. *J. Neurophysiol.* **76**, 3656-3665 (1996). https://doi.org/10.1152/jn.1996.76.6.3656

9 Han, Z. S., Zhang, E. T. & Craig, A. D. Nociceptive and thermoreceptive lamina I neurons are anatomically distinct. *Nat. Neurosci.* **1**, 218-225 (1998). https://doi.org/10.1038/665

10 Carta, M., Vestergaard, M. & Poulet, J. F. A. The neuronal circuits and cellular encoding of thermosensation. *Nat. Rev. Neurosci.* (2025). https://doi.org/10.1038/s41583-025-01001-5

11 Roome, R. B. *et al.* Phox2a Defines a Developmental Origin of the Anterolateral System in Mice and Humans. *Cell Rep.* **33**, 108425 (2020). https://doi.org/10.1016/j.celrep.2020.108425

12 Alsulaiman, W. A. A. *et al.* Characterisation of lamina I anterolateral system neurons that express Cre in a Phox2a-Cre mouse line. *Sci Rep* **11**, 17912 (2021). https://doi.org/10.1038/s41598-021-97105-w

13 Polgár, E., Wright, L. L. & Todd, A. J. A quantitative study of brainstem projections from lamina I neurons in the cervical and lumbar enlargement of the rat. *Brain Res.* **1308**, 58-67 (2010). https://doi.org/10.1016/j.brainres.2009.10.041

14 Osseward, P. J., 2nd *et al.* Conserved genetic signatures parcellate cardinal spinal neuron classes into local and projection subsets. *Science* **372**, 385-393 (2021). https://doi.org/10.1126/science.abe0690

15 Wercberger, R., Braz, J. M., Weinrich, J. A. & Basbaum, A. I. Pain and itch processing by subpopulations of molecularly diverse spinal and trigeminal projection neurons. *Proc. Natl. Acad. Sci.* **118**, e2105732118 (2021). https://doi.org/10.1073/pnas.2105732118

16 Alsulaiman, W. A. A. *et al.* Characterisation of lamina I anterolateral system neurons that express Cre in a Phox2a-Cre mouse line. *Sci. Rep.* **11**, 17912 (2021). https://doi.org/10.1038/s41598-021-97105-w

17 Menetrey, D., De Pommery, J., Thomasset, M. & Baimbridge, K. G. Calbindin-D28K (CaBP28k)-like Immunoreactivity in Ascending Projections. *Eur J Neurosci* **4**, 70-76 (1992). https://doi.org/10.1111/j.1460-9568.1992.tb00110.x

18 Choi, S. *et al.* Parallel ascending spinal pathways for affective touch and pain. *Nature* **587**, 258-263 (2020). https://doi.org/10.1038/s41586-020-2860-1

19 Hachisuka, J., Koerber, H. R. & Ross, S. E. Selective-cold output through a distinct subset of lamina I spinoparabrachial neurons. *PAIN* **161**, 185-194 (2020). https://doi.org/10.1097/j.pain.0000000000001710

20 Huang, T. *et al.* Identifying the pathways required for coping behaviours associated with sustained pain. *Nature* **565**, 86-90 (2019). https://doi.org/10.1038/s41586-018-0793-8

21 Ma, Q. A functional subdivision within the somatosensory system and its implications for pain research. *Neuron* **110**, 749-769 (2022). https://doi.org/10.1016/j.neuron.2021.12.015

22 Zhang, M.-D. *et al.* Neural ensembles that encode nocifensive mechanical and heat pain in mouse spinal cord. *Nat. Neurosci.*, 1-12 (2025). https://doi.org/10.1038/s41593-025-01921-6

23 Wang, F. *et al.* Sensory Afferents Use Different Coding Strategies for Heat and Cold. *Cell Rep.* **23**, 2001-2013 (2018). https://doi.org/10.1016/j.celrep.2018.04.065

24 Vestergaard, M., Carta, M., Güney, G. & Poulet, J. F. A. The cellular coding of temperature in the mammalian cortex. *Nature* **614**, 725-731 (2023). https://doi.org/10.1038/s41586-023-05705-5

25 Bell, A. M. *et al.* Deep sequencing of Phox2a nuclei reveals five classes of anterolateral system neurons. *Proc Natl Acad Sci U S A* **121**, e2314213121 (2024). https://doi.org/10.1073/pnas.2314213121

26 Razlan, A. N. *et al.* https://doi.org/10.7554/eLife.109502.1

27 Wang, F. *et al.* Thermal and mechanical modalities converge in the noxious range. *bioRxiv*, 2025.2003.2003.641313 (2025). https://doi.org/10.1101/2025.03.03.641313

28 Takashima, Y. *et al.* Diversity in the neural circuitry of cold sensing revealed by genetic axonal labeling of transient receptor potential melastatin 8 neurons. *J Neurosci* **27**, 14147-14157 (2007). https://doi.org/10.1523/JNEUROSCI.4578-07.2007

29 Albisetti, G. W. *et al.* Identification of Two Classes of Somatosensory Neurons That Display Resistance to Retrograde Infection by Rabies Virus. *J Neurosci* **37**, 10358-10371 (2017). https://doi.org/10.1523/JNEUROSCI.1277-17.2017

30 Hachisuka, J. *et al.* Semi-intact ex vivo approach to investigate spinal somatosensory circuits. *eLife* **5**, e22866 (2016). https://doi.org/10.7554/elife.22866

31 Bodding, M., Wissenbach, U. & Flockerzi, V. Characterisation of TRPM8 as a pharmacophore receptor. *Cell Calcium* **42**, 618-628 (2007). https://doi.org/10.1016/j.ceca.2007.03.005

32 Albisetti, G. W. *et al.* Inhibitory Kcnip2 neurons of the spinal dorsal horn control behavioral sensitivity to environmental cold. *Neuron* **111**, 92-105 e105 (2023). https://doi.org/10.1016/j.neuron.2022.10.008

33 Lee, H. *et al.* A dedicated skin-to-brain circuit for cool sensation in mice. *Nat Commun* **16**, 6731 (2025). https://doi.org/10.1038/s41467-025-61562-y

34 Wang, H. *et al.* A novel spinal neuron connection for heat sensation. *Neuron* **110**, 2315-2333 e2316 (2022). https://doi.org/10.1016/j.neuron.2022.04.021

35 Bourane, S. *et al.* Gate control of mechanical itch by a subpopulation of spinal cord interneurons. *Science* **350**, 550-554 (2015). https://doi.org/10.1126/science.aac8653

36 Paricio-Montesinos, R. *et al.* The Sensory Coding of Warm Perception. *Neuron* **106**, 830-841.e833 (2020). https://doi.org/10.1016/j.neuron.2020.02.035

37 Milenkovic, N. *et al.* A somatosensory circuit for cooling perception in mice. *Nat. Neurosci.* **17**, 1560-1566 (2014). https://doi.org/10.1038/nn.3828

38 Mishra, S. K., Tisel, S. M., Orestes, P., Bhangoo, S. K. & Hoon, M. A. TRPV1-lineage neurons are required for thermal sensation. *EMBO J.* **30**, 582-593 (2011). https://doi.org/10.1038/emboj.2010.325

39 Britz, O. *et al.* A genetically defined asymmetry underlies the inhibitory control of flexor-extensor locomotor movements. *eLife* **4** (2015). https://doi.org/10.7554/eLife.04718

40 Reimúndez, A. *et al.* Deletion of the Cold Thermoreceptor TRPM8 Increases Heat Loss and Food Intake Leading to Reduced Body Temperature and Obesity in Mice. *J. Neurosci.* **38**, 3643-3656 (2018). https://doi.org/10.1523/jneurosci.3002-17.2018

41 Škop, V. *et al.* Mouse Thermoregulation: Introducing the Concept of the Thermoneutral Point. *Cell Rep.* **31**, 107501 (2020). https://doi.org/10.1016/j.celrep.2020.03.065

42 Baldo, M. B., Antenucci, C. D. & Luna, F. Effect of ambient temperature on evaporative water loss in the subterranean rodent Ctenomys talarum. *J Therm Biol* **53**, 113-118 (2015). https://doi.org/10.1016/j.jtherbio.2015.09.002

43 Thomas, S. A. & Palmiter, R. D. Thermoregulatory and metabolic phenotypes of mice lacking noradrenaline and adrenaline. *Nature* **387**, 94-97 (1997). https://doi.org/10.1038/387094a0

44 Leva, T. *et al.* The cellular representation of temperature across the somatosensory thalamus. *bioRxiv*, 2024.2002.2013.580167 (2024). https://doi.org/10.1101/2024.02.13.580167

45 Craig, A. D. & Blomqvist, A. Is there a specific lamina I spinothalamocortical pathway for pain and temperature sensations in primates? *J Pain* **3**, 95-101; discussion 113-104 (2002). https://doi.org/10.1054/jpai.2002.122953

46 Bokiniec, P., Whitmire, C. J. & Poulet, J. F. A. Bidirectionally responsive thermoreceptors encode cool and warm. *bioRxiv*, 2024.2011.2028.625856 (2024). https://doi.org/10.1101/2024.11.28.625856

47 Yahiro, T., Kataoka, N., Nakamura, Y. & Nakamura, K. The lateral parabrachial nucleus, but not the thalamus, mediates thermosensory pathways for behavioural thermoregulation. *Sci Rep* **7**, 5031 (2017). https://doi.org/10.1038/s41598-017-05327-8

48 Yang, W. Z. *et al.* A parabrachial-hypothalamic parallel circuit governs cold defense in mice. *Nat Commun* **14**, 4924 (2023). https://doi.org/10.1038/s41467-023-40504-6

49 Vandewauw, I. *et al.* A TRP channel trio mediates acute noxious heat sensing. *Nature* **555**, 662-666 (2018). https://doi.org/10.1038/nature26137

50 Tan, C. L. & Knight, Z. A. Regulation of Body Temperature by the Nervous System. *Neuron* **98**, 31-48 (2018). https://doi.org/10.1016/j.neuron.2018.02.022

51 Bourane, S. *et al.* Identification of a Spinal Circuit for Light Touch and Fine Motor Control. *Cell* **160**, 503-515 (2015). https://doi.org/10.1016/j.cell.2015.01.011

931 52 Zhang, X., Millecamps, M. & Kania, A. Genetic evidence of the function of Phox2a-
932 expressing anterolateral system neurons in the transmission of chronic pain. *Mol. Pain* **19**,
933 17448069231170546 (2023). https://doi.org/10.1177/17448069231170546

934 53 Bourojeni, F. B., Zeilhofer, H. U. & Kania, A. Netrin-1 receptor DCC is required for the
935 contralateral topography of lamina I anterolateral system neurons. *PAIN* **162**, 161-175
936 (2021). https://doi.org/10.1097/j.pain.0000000000002012

937 54 Kohro, Y. *et al.* A new minimally-invasive method for microinjection into the mouse spinal
938 dorsal horn. *Sci. Rep.* **5**, 14306 (2015). https://doi.org/10.1038/srep14306

939 55 Ganley, R. P. *et al.* Inhibitory Interneurons That Express GFP in the PrP-GFP Mouse Spinal
940 Cord Are Morphologically Heterogeneous, Innervated by Several Classes of Primary
941 Afferent and Include Lamina I Projection Neurons among Their Postsynaptic Targets. *J*
942 *Neurosci* **35**, 7626-7642 (2015). https://doi.org/10.1523/JNEUROSCI.0406-15.2015

943 56 Ward, J. H. Hierarchical Grouping to Optimize an Objective Function. *J Am Stat Assoc* **58**,
944 236-& (1963). https://doi.org/Doi 10.2307/2282967

945 57 Laffray, S. *et al.* Adaptive movement compensation for in vivo imaging of fast cellular
946 dynamics within a moving tissue. *PLoS One* **6**, e19928 (2011).
947 https://doi.org/10.1371/journal.pone.0019928

948 58 Moqrich, A. *et al.* Impaired thermosensation in mice lacking TRPV3, a heat and camphor
949 sensor in the skin. *Science* **307**, 1468-1472 (2005).
950 https://doi.org/10.1126/science.1108609

951 59 Bonin, R. P., Bories, C. & De Koninck, Y. A simplified up-down method (SUDO) for
952 measuring mechanical nociception in rodents using von Frey filaments. *Mol Pain* **10**, 26
953 (2014). https://doi.org/10.1186/1744-8069-10-26

954 60 Pan, H. *et al.* Identification of a Spinal Circuit for Mechanical and Persistent Spontaneous
955 Itch. *Neuron* **103**, 1135-1149 e1136 (2019). https://doi.org/10.1016/j.neuron.2019.06.016

956 61 Mogil, J. S. *et al.* Heritability of nociception I: responses of 11 inbred mouse strains on 12
957 measures of nociception. *PAIN* **80**, 67-82 (1999). https://doi.org/10.1016/s0304-
958 3959(98)00197-3

959 62 Colburn, R. W. *et al.* Attenuated cold sensitivity in TRPM8 null mice. *Neuron* **54**, 379-386
960 (2007). https://doi.org/10.1016/j.neuron.2007.04.017

961 63 Friard, O., Gamba, M. & Fitzjohn, R. BORIS: a free, versatile open-source event-logging
962 software for video/audio coding and live observations. *Methods in Ecology and Evolution*
963 **7**, 1325-1330 (2016). https://doi.org/10.1111/2041-210x.12584

64 Walsh, R. N. & Cummins, R. A. The open-field test: A critical review. *Psychological Bulletin* **83**, 482-504 (1976). https://doi.org/10.1037/0033-2909.83.3.482

65 Paxinos, G. & Franklin, K. B. J. *The mouse brain in stereotaxic coordinates*. 2nd edn, (Academic Press, 2001).